2015-01-01

Lithospheric Structure And Stress Field Orientations In The Northern Libya And East-Central Mediterranean Region

Abdusalam Ali Agail
University of Texas at El Paso, aaagail@miners.utep.edu

LITHOSPHERIC STRUCTURE AND STRESS FIELD ORIENTATIONS IN THE NORTHERN LIBYA AND EAST-CENTRAL MEDITERRANEAN REGION

ABDUSALAM ALI OMAR AGAIL, MSc

Department of Geological Sciences

APPROVED:

_____
Diane Doser, Ph.D., Chair

_____
Aaron Velasco, Ph.D.

_____
Philip Goodell, Ph.D.

_____
Richard Langford, Ph.D.

_____
Mohamed Khamsi, Ph.D.

_____
Charles Ambler, Ph.D.
Dean of the Graduate School

Dedication

To my mother

Salmah Alabed

LITHOSPHERIC STRUCTURE AND STRESS FIELD ORIENTATIONS IN THE NORTHERN LIBYA AND EAST-CENTRAL MEDITERRANEAN REGION

by

ABDUSALAM ALI OMAR AGAIL

THESIS

Presented to the Faculty of the Graduate School of

The University of Texas at El Paso

In Partial Fulfillment

Of the Requirements

for the Degree of

DOCTOR OF PHILOSOPHY

Department of Geological Sciences

THE UNIVERSITY OF TEXAS AT EL PASO

December 2015

ACKNOWLEDGEMENTS

I would like to express my great gratitude and sincere thanks to my committee chair, Dr. Diane Doser, for her support and guidance. I am very thankful to her effort that made it possible for me to accomplish my work. My deepest thanks and appreciation to Dr. Aaron Velasco for his advice during my work. A special thanks goes also to my committee Dr. Philip Goodell, Dr. Richard Langford, and Dr. Khamsi Amine. I would like also to extend my thanks to the department of Geological Sciences-UTEP for their support. My great appreciation and thanks goes also to the following people and institutions for their help and contributions: The Libyan National Seismological Network (LNSN), Tripoli, Libya for providing the data and facilitating my work, Abdala Elmelade (The Head of Department of Research and Field Studies at the LNSN) along with Amir Sharif, Fathi Belead, and Muhammad Salah for their help in getting my data. In addition, I also thank the SEISAN group (Jens Havskov and Lars Ottemöller, Department of Earth Sciences, University of Bergen, Norway) for helping answering questions regarding the data and software.

ABSTRACT

This thesis is a combination of three studies including tomography using surface wave group velocities, stress orientations from focal mechanisms, and receiver functions. The study area covers northern Libya and the east central Mediterranean region. I utilized new data from the Libyan National Seismic Network to better understand the crustal thickness and stress orientation of northern Libya as well as the east central Mediterranean region.

In the first study, I conducted surface wave group velocity tomography implementing the Gaussian beam method for obtaining 2-D velocity variations assuming an isotropic model. I constructed surface wave group velocity maps over a range of periods for both Love and Rayleigh waves on a 2.0° x 2.0° grid. The results resolved the main geological features in the central Mediterranean and northern Libya. Crustal thickness variation of the Libyan margins shows a gradient (South to North) interpreted as a change from continental to oceanic crust. A thinner crust was resolved in the central Mediterranean beneath the Ionian Sea and Abyssal Plan. The Hellenic subduction zone and the Calabrian Accretionary prism were imaged as zones with very low group velocities.

In the second study, 10 new focal mechanism solutions are presented and a total of 26 focal mechanisms from local earthquakes in northern Libya were used in an inversion to determine the variation of principles stress of the northern Libya area. The results indicate that there are two different regional stress orientations. In Zone I (north central Libya) the maximum principal stress orientation ($\sigma 1$) has a strike 95° and plunge of 22°. The orientation of the greatest principal stress ($\sigma 1$) in Zone II (northeastern Libya, Cyrenaica region) has a strike of 327° and plunge of 13°. In Zone III (northwestern Libya), $\sigma 1$ has a strike of 129° and plunge of 16°. These results show a rotation of the maximum principal stress orientation from southeast in

northwestern Libya to northwest in eastern Libya. This confirms the existence of at least two different stress regimes in the area, which has been suggested by previous studies.

In the third study, I analyzed waveforms from 66 teleseismic events (distances of 4000 km to 15700 km and magnitudes of 0.1 to 4.5) to compute receiver functions using a frequency - domain method that is based on the deconvolution of the vertical components. Unfortunately, due to the lack of well-recorded data I was not able to obtain viable receiver functions results. More data are required to adequately determining these receiver functions.

TABLE OF CONTENTS

LIST OF TABLES

LIST OF FIGURES

INTRODUCTION

The first goal of this study is to integrate different geophysical methods including surface wave dispersion and receiver functions to better determine the crustal thickness in northern Libya and the east-central Mediterranean. A second goal is to determine source parameters of earthquakes and crustal structure of northern Libya. This integrated study will assist in understanding the distribution of the seismicity and seismotectonics within the study area. This study is one of the first to investigate the seismic data recorded by new stations of the Libyan National Seismic Network (LNSN) operating in Libya since 2005.

We hope in this study to contribute to the general picture of geology, tectonics, and geodynamics of the area. Our goal is to provide a greater understanding of the crustal structure within the central Mediterranean and beneath the Libyan region. Improving the estimates of the crustal structure is essential for forming a greater understanding of the region's geodynamic evolution, deformation and seismicity. In addition, the oceanic-continent transition north of Libya is critical for understanding and evaluating petroleum systems associated with this region.

CHAPTER 1: TOMOGRAPHY OF SURFACE WAVE-GROUP VELOCITY

1.1 INTRODUCTION:

The Mediterranean region is a geologically complex area due to its geodynamic evolution and its position near the boundary between the Eurasian and African plates. The central and eastern Mediterranean is of Mesozoic and Cenozoic ages (Carminati 2004). This region is characterized by deep basins and mountain belts, which have been created by the convergence of the African, Arabian, and Eurasian plates. The development of the Mediterranean and Tethys Oceans had a primary effect on the tectonics of Libya during the Mesozoic and Cenozoic. Early tectonism in Libya was controlled by the evolution of Gondwana and Pangaea within the Palaeozoic and Mesozoic. In addition, inter-plate deformation has significantly affected the tectonics in Libya. Seismic activity is mostly observed in the northwest part of Libya (Al-Heety 2006).

The convergence of Africa, Arabia, and Eurasia has been active since the late Cretaceous (Vannucci et al., 2004). This tectonic activity has led to wide variations in estimates of Moho depth (between 15 km to 45 km). The uncertainties in crustal thickness are higher along the northern coast of Africa (Van der Meijde et al., 2003). Furthermore, this region is seismically active as a result of rapid deformation. Geodynamic studies reveal a complex pattern of contrasting tectonic features including compressive, extensional, and strike-slip regimes coexisting together. The Hellenic subduction zone is located in the east central Mediterranean where the African plate is converging beneath the Eurasian plate. This subduction zone extends for about 1000 km from the southern Mediterranean to the Ionian Sea. The reported rate motion of the plates along the Hellenic zone is ~ 35 ± 1 mm yr^{-1} (McClusky et al., 2003). The crust beneath the Ionian Abyssal plain (fig.1.01) has a typical oceanic structure with a Moho depth of

16-18 km. In the westward direction and toward the Malta escarpment the crust thickens and becomes more continental. The Ionian crust varies from 17-22 km in thickness and is covered by sedimentary layers ~ 8 km thick (Sartori 2003, Rosenbaum 2004, and Gallais et al., 2011). The thin crust of the Ionian basin beneath the Ionian Sea has been interpreted as an oceanic crust (Gallais et al., 2011).

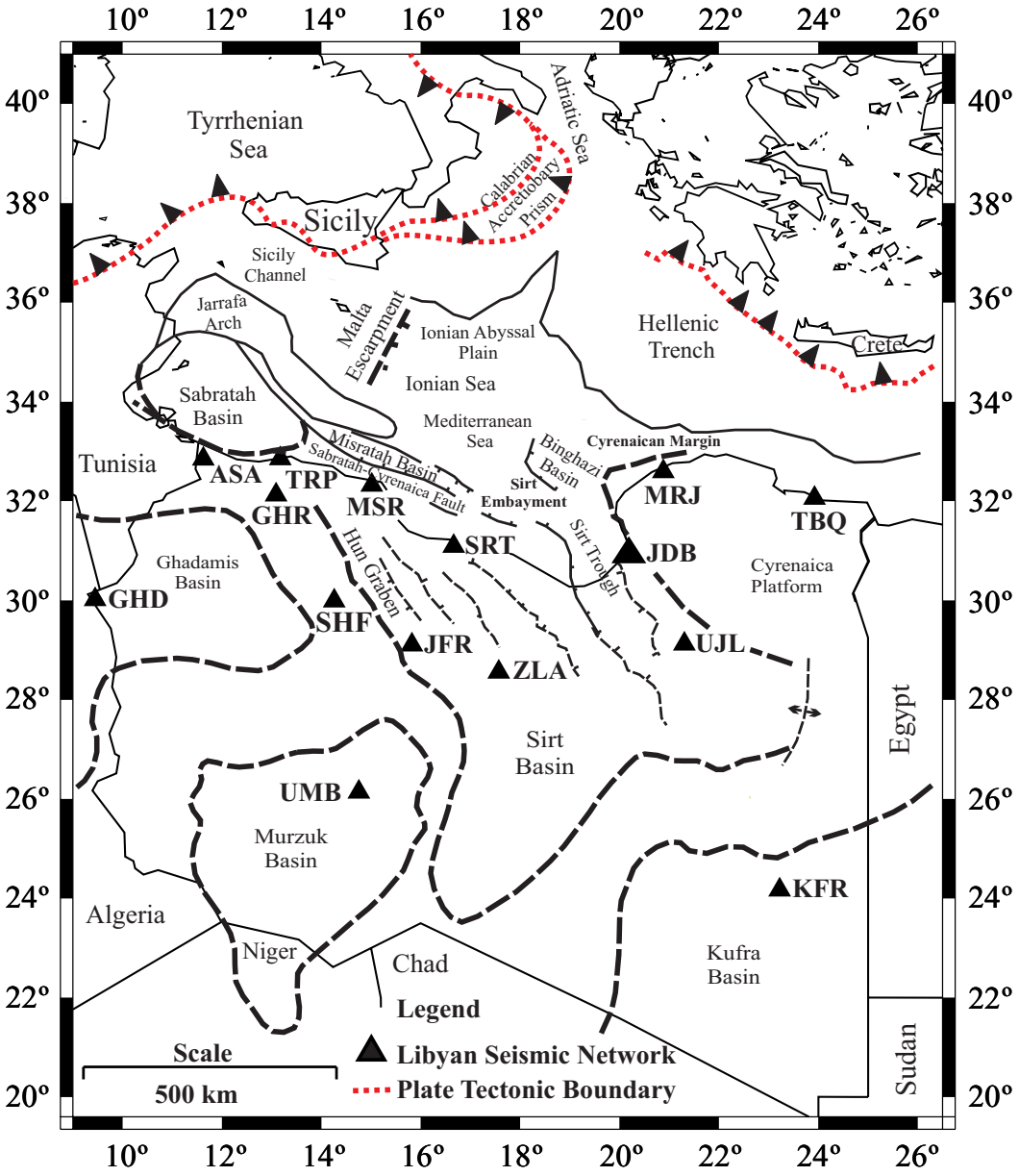

Figure 1.01: Regional geologic setting of the study area as well as stations of the Libyan National Seismic Network (LNSN) used in this study.

Crustal thickness and velocity have been targets for many studies in the Mediterranean as well as the Libyan region (e.g., Sandvol et al., 1998; Van der Meijde et al., 2003, 2005; Marone et al 2004; Pasyanos & Nyblade 2007; Pasyanos, 2010; Roure et al, 2012). Although the structure of the Libyan offshore margin may be better known based on seismic reflection profiles, many issues still need to be addressed. In addition, little petroleum related information has been released, especially in northern Libya, making it very challenging to obtain a good understanding of the geology in the region (Roure et al., 2012). A recent gravity study by Cowie and Kusznir (2012) concluded that a highly thinned continental crust is predicted beneath the offshore Sirte basin (15 km). In contrast, a very thin oceanic crust is predicted by the gravity inversion beneath the Ionia Sea (Cowie and Kusznir, 2012). These issues have been emphasized in previous studies and are mainly related to a number of problems such as sparse coverage of geophysical data, lack of data, and uneven distribution of seismograph stations within the region.

This dissertation uses seismic tomography based on surface wave group velocity variations as a tool for resolving the changes in crustal thickness and composition present in the area and their relation to ongoing geologic processes. There have been many recent surface wave tomography studies in the northern portion of the central-eastern Mediterranean e.g. (Piromallo and MoreIll, 1997; Martinez et al. 2000; Hazler et al., 2001; Pasyanos & Walter 2002; Karagianni et al., 2002; Piromallo and Morelli, 2003; Boschi et al., 2004: Meier. et al., 2004: Pasyanos 2005; Lucio & Pasyanos 2007; Schivardi and Morelli, 2009). However, these previous studies have not utilized any data recorded by the LNSN and consequently have not been able to adequately resolve the structure of offshore and onshore Libya.

1.2 DATA:

This study uses waveform data from the Libyan National Seismological Network (LNSN). This network is operated by the Libyan Center for Remote Sensing and Space Science, Tripoli, Libya. This network consists of two previously operating broadband seismographs (GHR (GHAR) and MRJ (MARJ)) and 13 newer stations. The sampling rate of the stations is 40 -100 samples/sec. The instruments have an operating bandwidth of 0.1 Hz to 85.5 Hz. A total of 68 regional events from 2008-2010 recorded by the LNSN were used in this study (see the appendix for details about the events). These events are mainly concentered on the plate boundary especially in the Hellenic subduction zone. The ray paths for these selected events cover most of northern Libya and the east central Mediterranean (Ionian Sea, offshore Libya) (fig. 1.02).

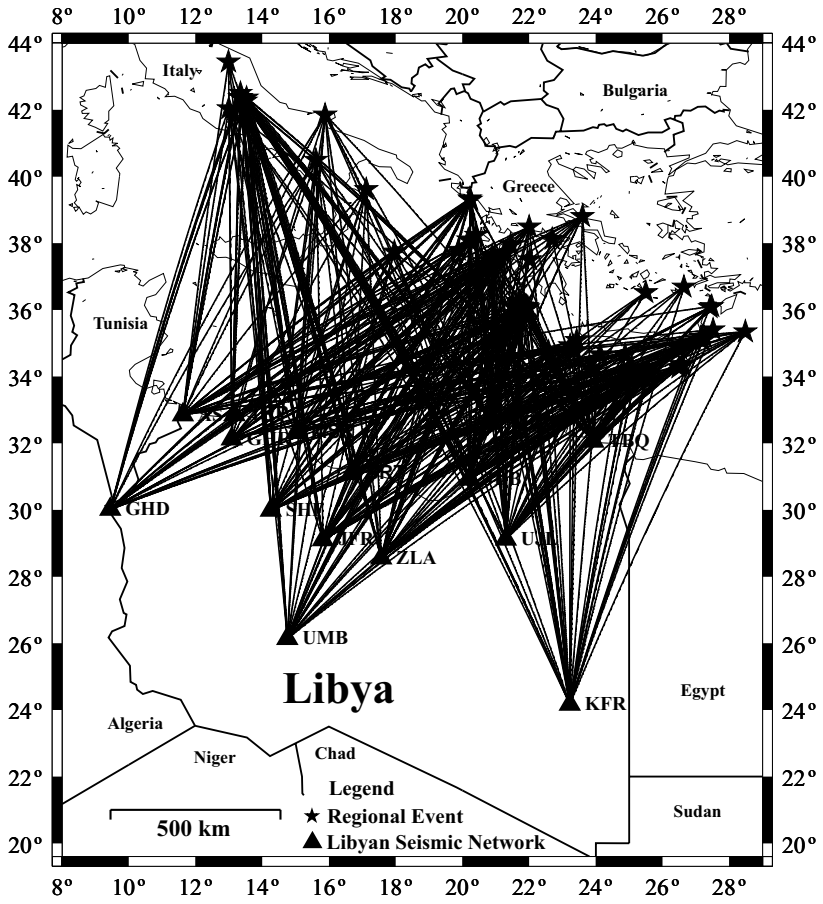

Figure 1.02: Ray coverage map.

The raw seismic data was received in SEISAN (seismic analysis system) format (Ottemoller et al., 2013). We first converted the data into SAC (Seismic Analysis Code) format using the "wavetool" program implemented in SEISAN. Header information was then added into the SAC waveform files. The header information had to be updated. The events locations, magnitudes, and depths were taken from the reviewed Bulletin of the International Seismic Center (ISC). In addition, SAC response files were created for each station using PDCC (Portable Data Collection Center) software.

1.3 METHODS:

1.3.1 Group velocity measurements:

We computed displacement seismograms for the selected events and then group velocity dispersion curves were obtained using the PGSWMFA (PGplot Surface Wave Multiple Filter Analysis) code designed by Ammon (2001). Applying a Gaussian filter width parameter of 10 on the selected components and then picking the maximum amplitude of the envelope function was used to compute the group velocity. The arrival time of the amplitude was used to calculate the group velocity (Herrmann, 1973). The number of dispersion measurements for each period is shown in (fig. 1.03). The dispersion curves were obtained for selected periods of 5-150 seconds for velocity ranges between 2.5 to 4.75 km/s.

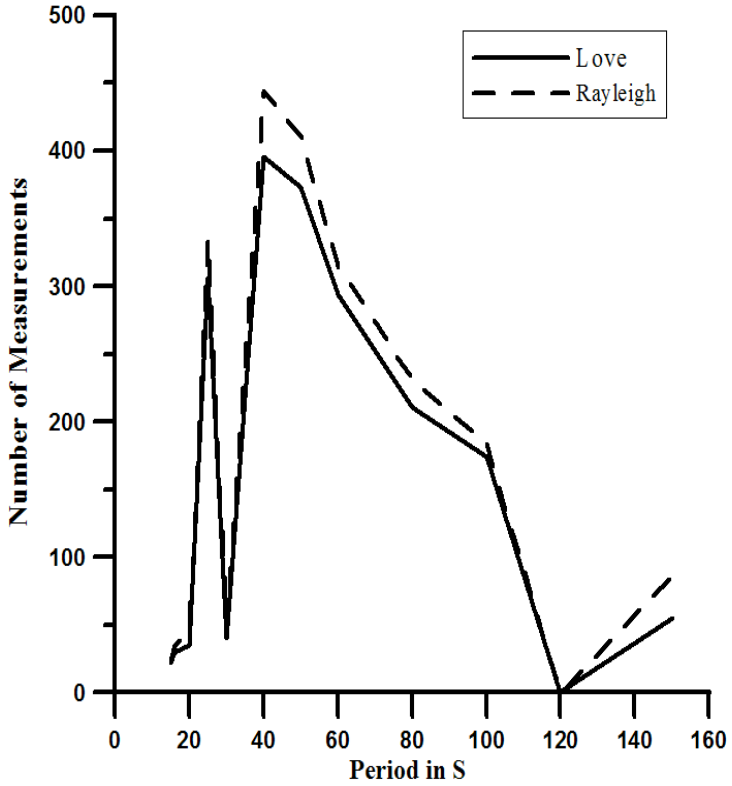

Figure 1.03: Group velocity measurements obtained in this study.

1.3.2 Tomography inversion:

We applied the tomographic method of Barmin et al. (2001), which uses the Gaussian beam method for obtaining the 2-D tomographic maps for group velocity variations assuming a constant isotropic velocity model. This method provides fast and robust tomographic maps on regional and global scales and has been extensively used in many studies.

1.3.3 Data errors:

Uncertainties in group velocity measurements can arise from different sources. First, some errors may result from uneven path distributions that cause uneven sampling of velocity variations. Second, other errors may be caused by assumptions made such as input parameters in the inversion processes. Here we implemented the method used by Schivardi and Morelli (2009) to estimate data errors. This method assumes that the measured group velocity in a cluster of

events should be the same. We selected 6 clusters to examine. Each cluster has 2-6 events all located within 10 km of each other. These clusters are shown in (fig.1.04). We obtained the error by finding the average travel times for each cluster for different periods.

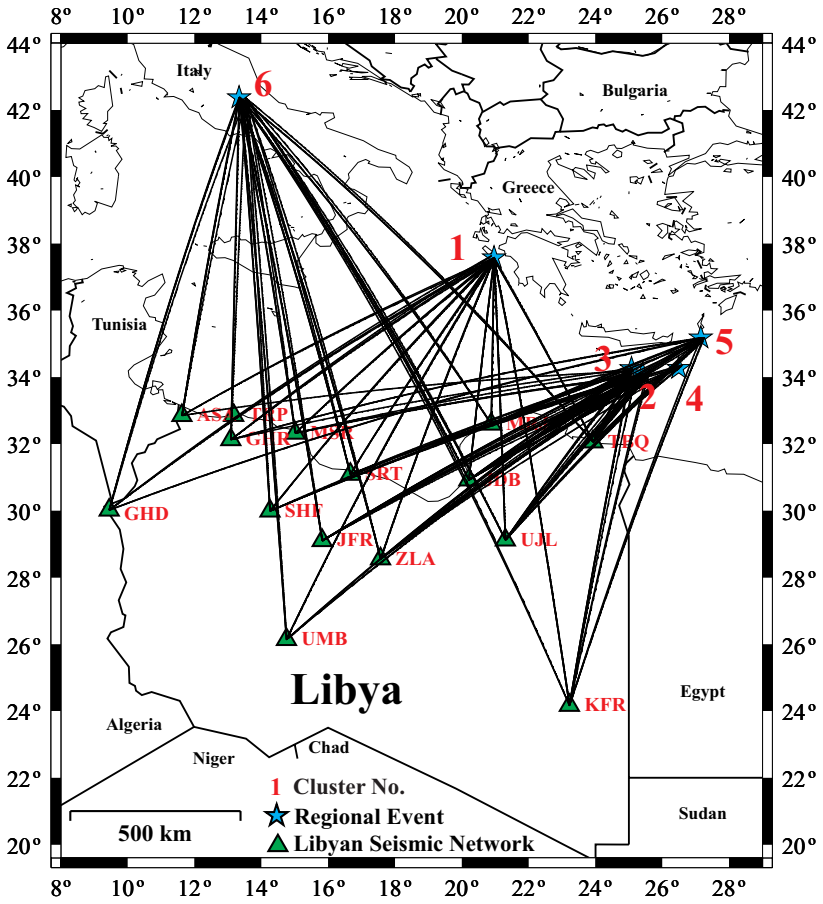

Figure 1.04: Clusters of events selected to measure the error in the group velocity.

Table 1.1: Example of some selected clustered events and the average measured group velocity. The error in travel time of group velocity is represented as standard deviation.

Events Cluster	Selected Stations	Periods	Group Velocity				Distance Km	Average Distance	Error in Time (STD)
			Event-1	Event-2	Event-3	Event-4			
Cluster-1	MRJ	35	3.7420	3.5870			1263.72 1272.69	1270.85	10
		40	3.8890	3.7010					8
		60	4.0520	3.9310					5
Cluster-2	TBQ	30	1.7810	2.3810	1.7600		267.10 260.48 258.85 249.06	258.87	18
		35	1.7950	2.4560	1.7600				19
		40	1.8300	2.5340	1.7600				20
		50	1.4950	1.8560	2.6450	1.7600			7

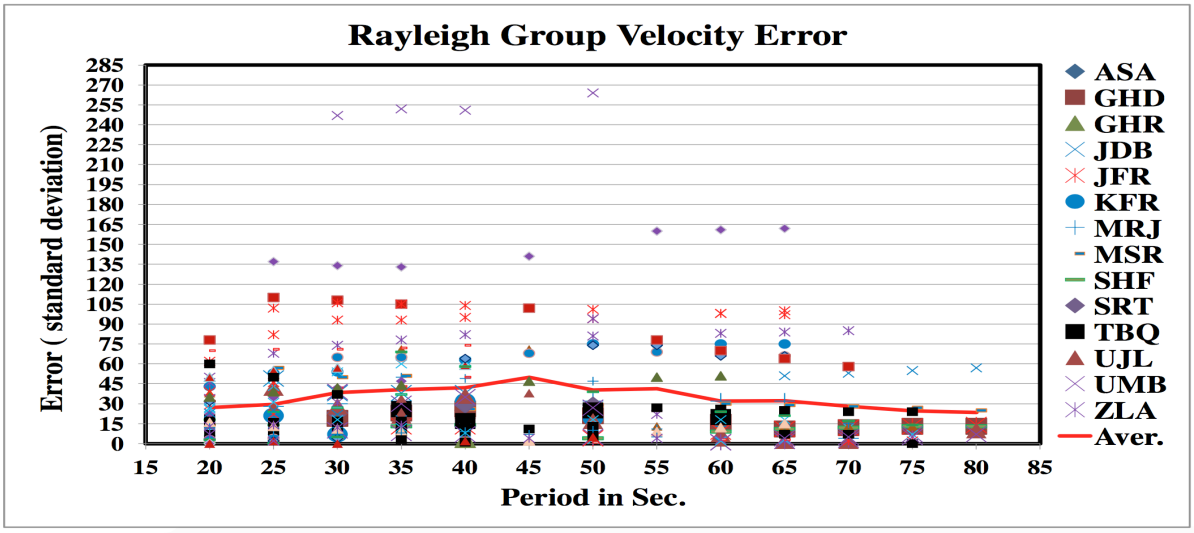

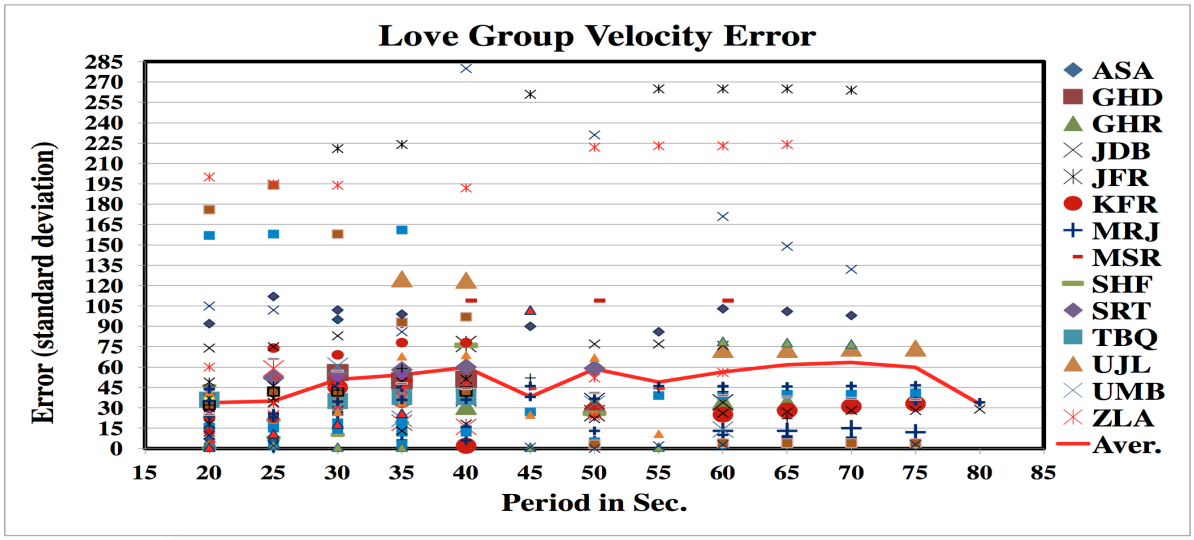

Figure 1.05: Love and Rayleigh group velocity travel time error results for each station as indicated by the symbols. The red curve is the average of all the group velocity measurements for a particular cluster.

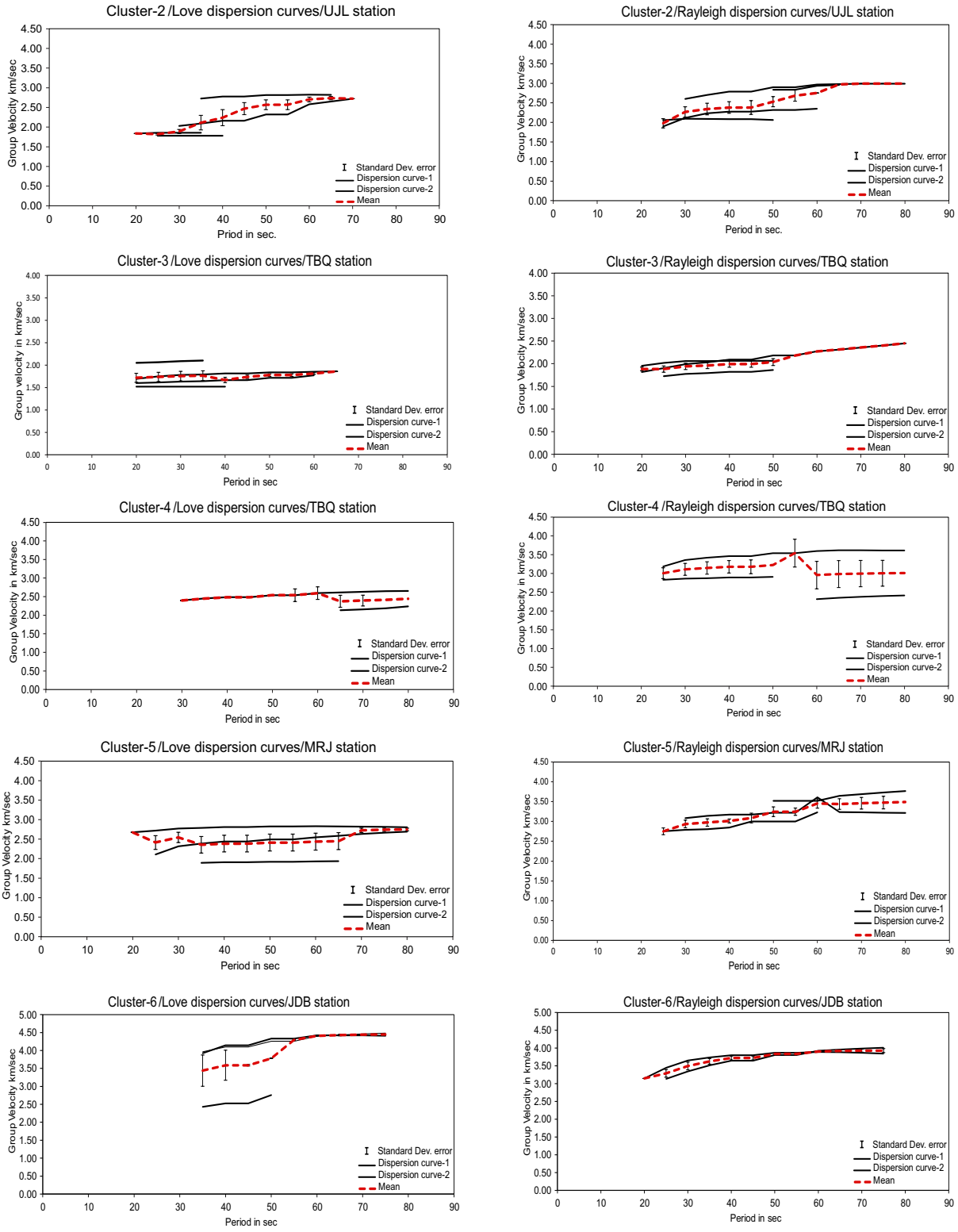

Figure 1.06: Dispersion curves for some cluster events selected to display the error in the group velocity measurements. The red dotted line shows the mean of the dispersion curves. Additional curves are shown in the appendix.

The results (fig. 1.05) show that the measured group velocities have higher values than expected. The average error of Love group velocity is 30 to 60 sec. The average error of Rayleigh group velocity is 25 to 45 sec. We believe that these high error values may be due to selecting the wrong event for the time window. Table 1.1 is an example that shows how misidentifying one event could greatly increase the standard deviation, which would lead to the higher error values obtained in (fig. 1.05).

These values are not representative of all the measured clusters. In addition to this method, we plotted the dispersion curves for some selected clustered events (fig. 1.06). The red dotted curve shows the mean of the dispersion curves for both Rayleigh and Love waves. The plotted dispersion curves presumably should show a very low deviation error on the graph. The shifted dispersion curves in some cases, which show a higher standard deviation error, reflect the error in the measured group velocity. Additional plotted dispersion curves are shown in the appendix.

1.4 RESULTS:

We constructed group velocity maps over a range of periods for both Love and Rayleigh waves on a 2.0° x 2.0° grid. Our focus here will be on periods between 20-80 sec due to the fact that most of our data fall within this range of periods. In this section and before proceeding to the tomographic maps we present here a simple method to test our inversion results.

1.4.1 Velocity variations:

The velocity variation in percentage shows that the biggest variation occurs at 20 sec for Rayleigh waves (fig. 1.07). The lowest velocity variation is in between periods of 40-60 sec. The maximum number of group velocities obtained is within the period of 40-60 sec.

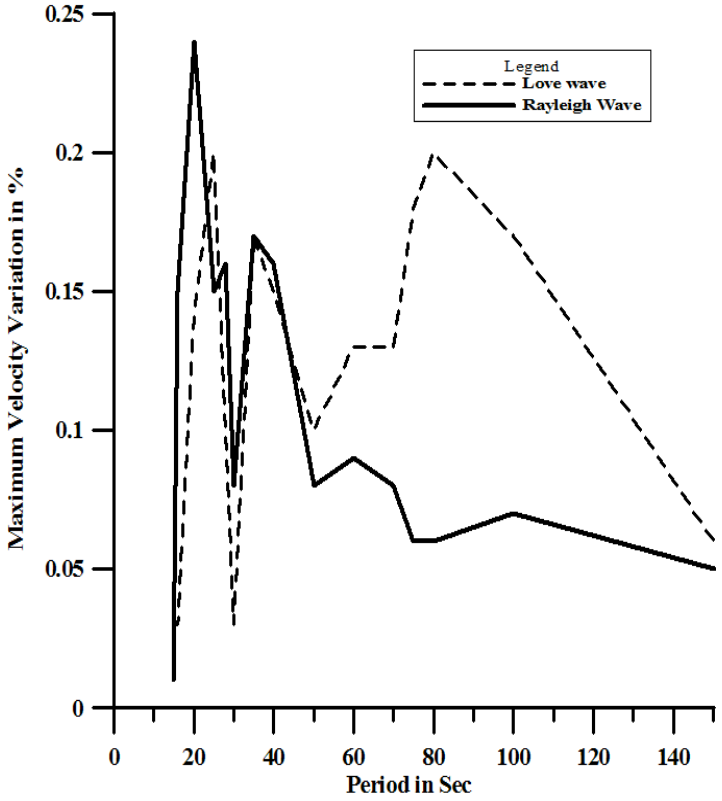

Figure 1.07: Velocity variations as a function of period.

1.4.2 Tomography results:

Generally, Love waves are more sensitive to shallow geological structures compared to Rayleigh waves recorded at the same period (Schivardi and Morelli 2009). The low group velocity at periods < 35 sec of both Love and Rayleigh waves are an indication of sedimentary basins. Rayleigh waves are more sensitive in this study, although Love waves with periods of 30 to 75 seconds generally are best at resolving crustal thickness. At periods of 100 sec Love waves sensitivity to sub-crustal structure increases (Ritzwoller et al., 1998). We will be comparing our results to the CRUST1.0 (Laske et al., 2013) model of depth to Moho and crustal thickness for the eastern Mediterranean (fig. 1.08).

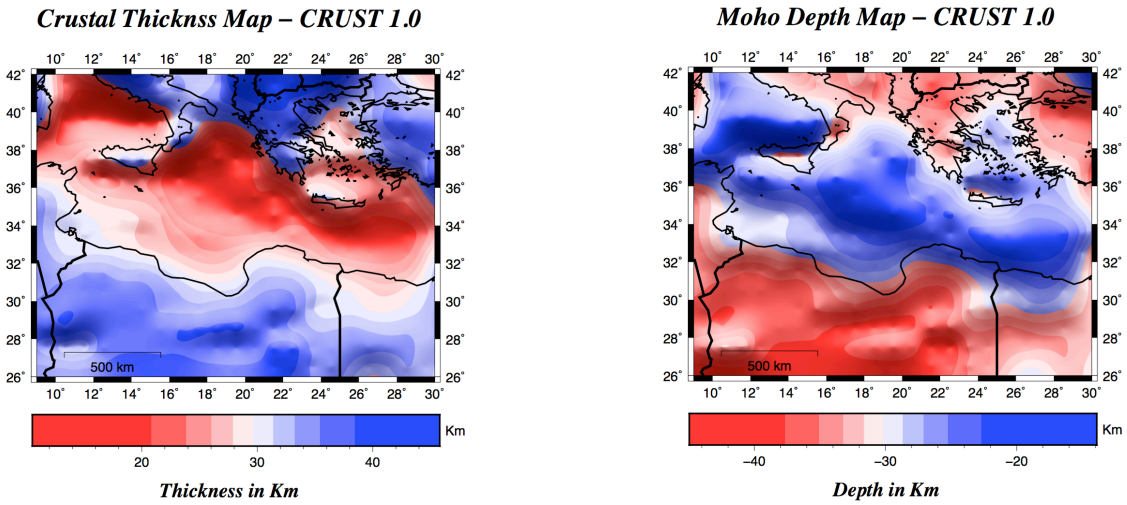

Figure 1.08: Crustal thickness and Moho depth map
CRUST1.0 model (Laske et al., 2013).

1.4.3.1 Crustal variation (continental-oceanic):

The crustal thickness variation is best observed at longer periods (above 50 sec) for both Rayleigh and Love waves (Ritzwoller et al., 1998). Short period surface waves (35-40 sec, Rayleigh; 35-60 sec Love) are sensitive to the difference in the crustal thickness (Schivardi and Morelli 2009). The low Rayleigh group velocity (2.1 to 3 km/sec) areas (yellow arrow) on maps at 30 and 37 sec (fig.1.09) mainly indicate regions of thicker continental crust. For Rayleigh waves with periods between 30 and 37 sec (fig. 1.09) we have interpreted the transition from low to high velocities as an indication of the crustal thinning in the direction of the yellow arrow on the map.

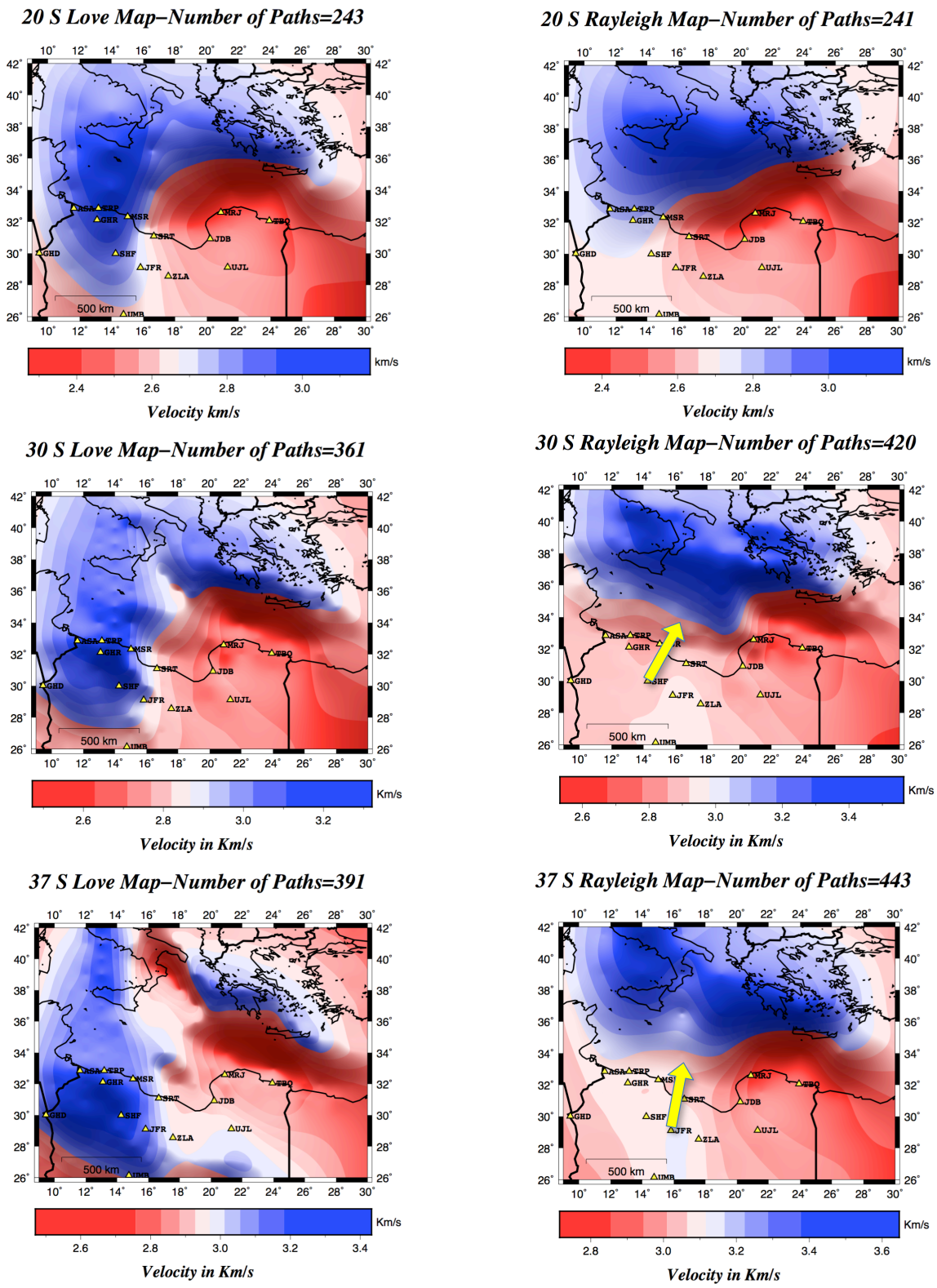

Figure 1.09: Selected tomographic maps from dispersion of group velocities (Love and Rayleigh waves). The yellow errors show the change of continental to oceanic crust.

At periods less than 30 sec Rayleigh and Love waves show similarity in group velocities where the only observed low group velocity structure is the Hellenic subduction zone. At periods of 30, 37, and 40 sec (fig. 1.09 and 1.10) Rayleigh waves in northern continental Libya show reduced group velocities between 2.9-3.2 km/sec, while they increase to 3.1-3.4 km/sec in the mid-northern Mediterranean. At 30 sec periods Rayleigh wave group velocities of 2.9-3.0 km/sec indicate thicker continental crust. Comparing these figures to the crustal thickness model (CRUST 1.0) of Laske et al. (2013) in (fig.1.08) we observe that a thinned continental crust (less than 25 km thick) is predicted to underlie the offshore Sirt basin and Ionian Sea (Cowie and Kusznir 2012). The dispersion signature of sedimentary structures, as well as increasing crustal thickness, can be seen on the 30, 37, and 40 sec plots of (fig. 1.09. & 1.10). A thin crustal layer (12-15 km thick) is found under the Ionian abyssal plain as was predicted by Kokinou et al. (2003).

In addition, the group velocity variations suggest the crust thins from the north to the south and that oceanic crust is being detected between the offshore Sirt basin and the Ionian Sea. Previously, Cowie and Kusznir (2012) suggested that this region contains oceanic crust or highly thinned continental crust (less than 20 km thick). Thin crust is also supported by Luccio & Pasyanos (2007). The observed low group velocity zone (at periods of 40 and 60) has been interpreted as an oceanic layer with subducted sediments. At longer periods (> 60 sec), especially for the Love wave maps of (fig. 1.10), we start to observe different group velocity variations where the continental crust is associated with higher group velocities in the continental part of Libya. In addition, we can observe the Hellenic and the Calabrian Accretionary prisms. In the central Mediterranean a lower velocity zone (2.2-2.9 km/sec) (fig. 1.10) extends from the eastern part of Libya towards the Hellenic Trench. This low group velocity zone has been interpreted as

representing the African oceanic lithosphere that has been subducted completely as the Hellenic Arc is closely approaching the African continental margin (Meier et al., 2004). In previous studies this has also been interpreted as sepentinized mantle in the subducting African plate (Suckale et al., 2009).

1.4.3.2 Crustal thickness:

Periods > 37 sec in the western part of Libya are characterized by a higher velocity zone (3.1-3.3 km/sec), which extends towards Sicily. In the eastern part of the Libyan region, a zone of low group velocity is clearly depicted. The sharp gradient in the 30 sec Love map (fig.1.09) indicates the shallowest crust is found beneath the Sirt Basin. The sediments in the offshore of Sirt basin are thicker than in the Ionian Sea, (Cowie and Kusznir 2012). By comparing this to the general crustal thickness map and Moho (fig. 1.08) depth we notice that there is a good match between crustal thickness and fast anomalies. At periods of 40 and 60 sec the Rayleigh waves that cross the Ionian Sea show a low group velocity zone. In addition, Love wave maps of periods of 37 and 40 sec show a gradient change in the crustal thickness where the thickness decreases towards the Ionian Sea and the abyssal plain. This matches very well with the gravity data reported by (Cowie and Kusznir 2012) where the reported thickness is about 35±10 km.

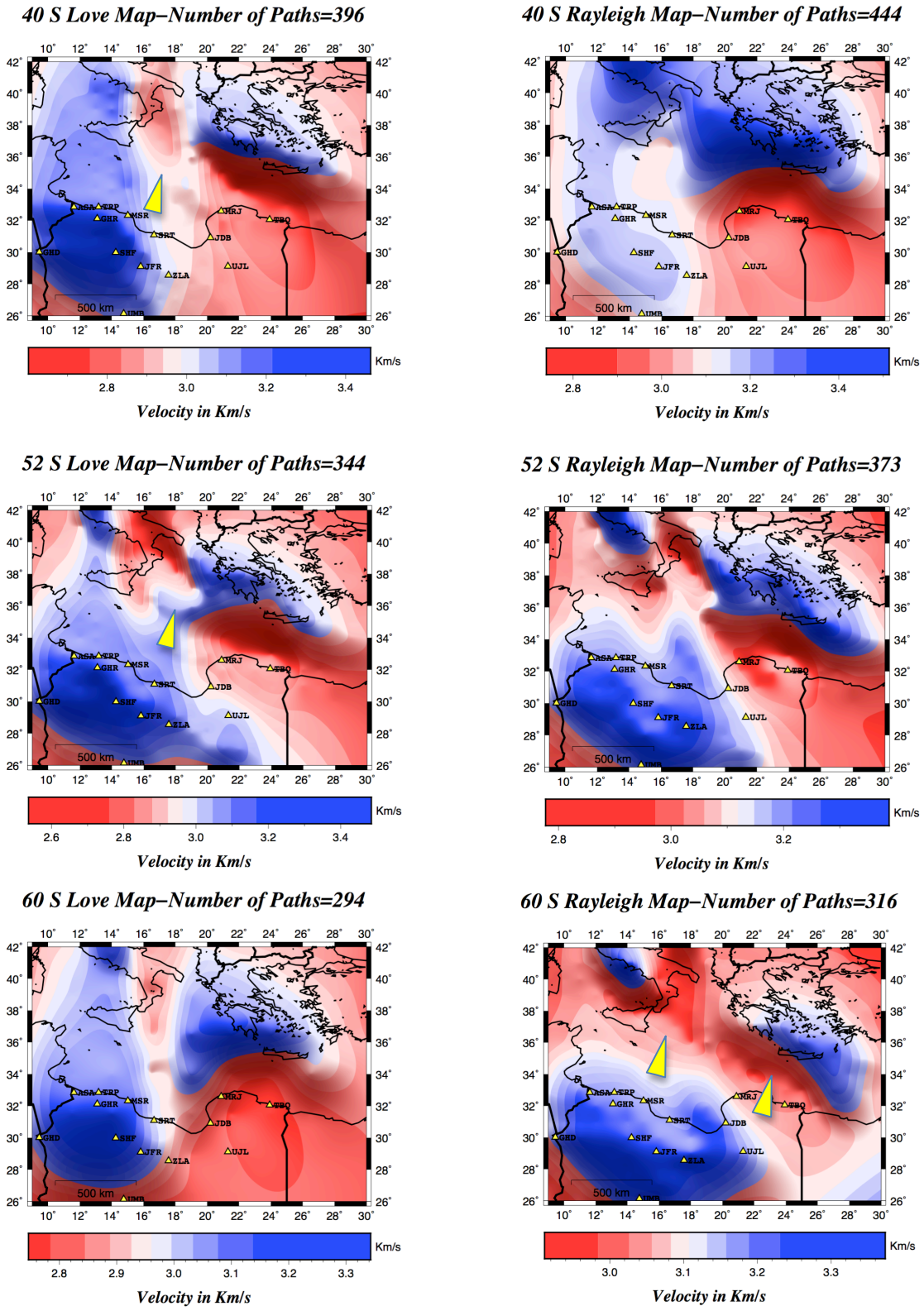

Figure 1.10: Tomographic inversion maps for Love and Rayleigh group velocities at periods of 40-75 sec. The yellow errors show the subduction zones and thinning crust.

1.4.3.3 Lithospheric structure:

To examine deeper lithospheric structure we need to examine the longer period Rayleigh waves (70 -75 sec). Since our group velocity measurements fall off above 70 sec (fig. 1.03) these maps are less accurate. On the 60, 70, and 75 sec Rayleigh maps (fig. 1.10) the abyssal plain and Calabrian Accretionary prisms are well delineated and are shown as low group velocity zones. The reported crustal thickness from the CRUST1.0 (Laske et al., 2013) model (fig 1.08) shows thicknesses of less than 20 km in this region. Schivardi et al. (2009) have indicated that it is an active area still evolving due to the collision of the two continents. In addition, the subducting plate of the Ionian Sea also appears as a low group velocity zone. According to Piana Agostinetti et al. (2009), an S-wave velocity profile showed a low velocity zone above the oceanic Ionian crust that they interpreted as sediments overlain on the Ionian oceanic crust.

1.4.4 Inversion testing:

To test our inversion results, we adopted a testing method that examines the uncertainty of the data involved in the inversion process (Doser et al., 1998). This method suggests that we can add random noise to the data and invert the noisy data to test the stability of the inversion. We added random noise of up to 10% to our group velocity data and we inverted these data to obtain results very similar to the original ones (fig. 1.11). If we added noise above ~17% this caused the inversion code to fail.

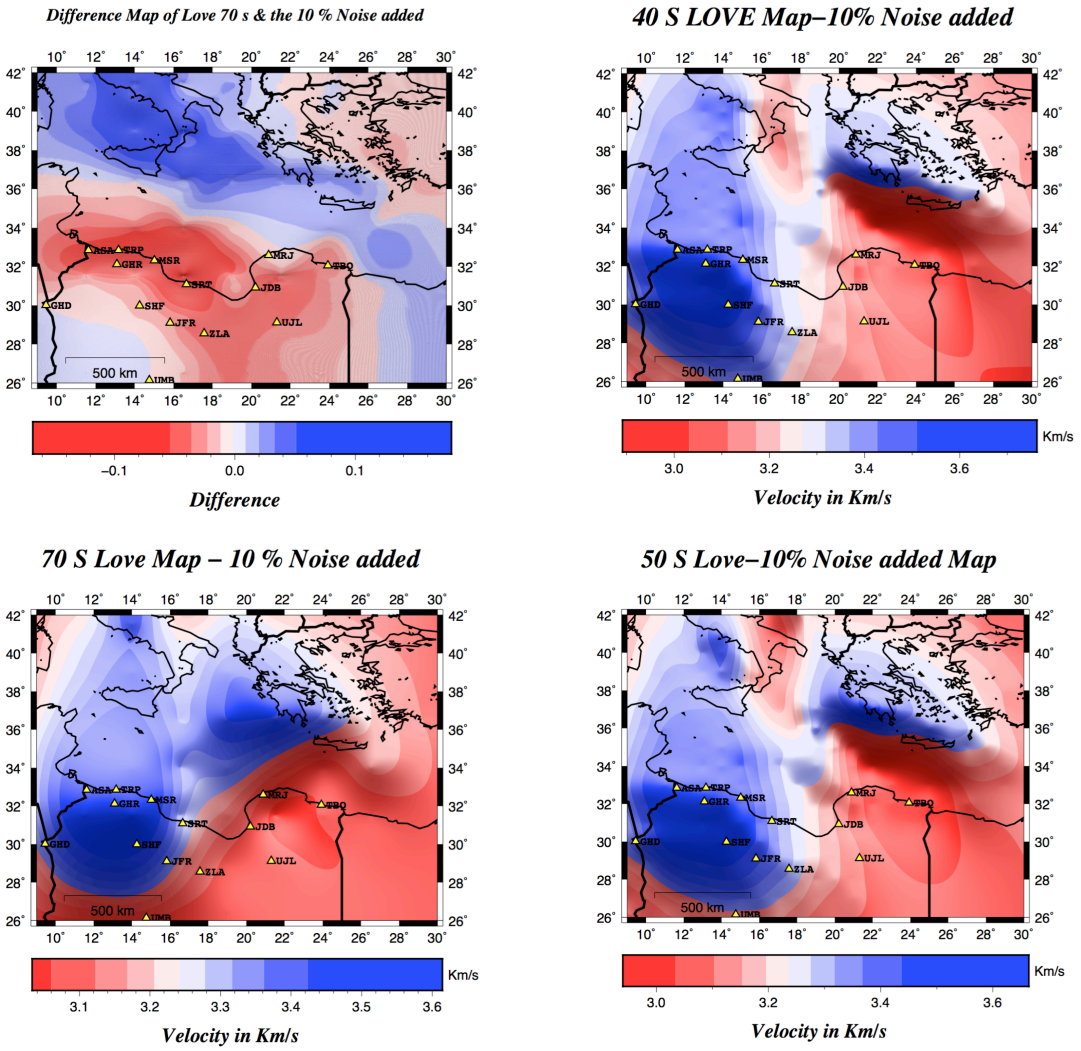

Figure 1.11: Results showing the difference between "noise free" inversions and inversions with 10% random noise added to the data.

1.5 DISCUSSION:

We calculated 68 Love and Rayleigh wave dispersion curves. The error results (fig. 1.05, 1.06 and appendix) showed that the errors were mainly caused by the selection of the wrong time window or wrong events. We produced 2D surface wave dispersion tomography maps assuming an isotropic model (reference model is constant) using the method of Barmin et al. (2001). Our results show that we can resolve the main crustal structures at periods between 40-70 s. In the

eastern Mediterranean the Hellenic subduction zone seems to be associated with a low group velocity zone at different periods. Although the data do not cover most of the study region and the ray path coverage is not relatively dense, some interesting features such as crustal variation (continental to oceanic crust) as well as crustal thickness changes were successfully mapped. Due to the fact we have a limited number of events and station converge we performed the tomographic inversion for a 2.0° x 2.0° grid. This resolution is too large to resolve many geological features of northwestern offshore Libya, for example the area of the Pelagian block (Sabarath basin).

In addition, observations of group velocities at short periods were very limited, making it also difficult to resolve these smaller scale features. However, the western part of Libya manifests itself as a region of higher group velocity (above 3.00 km/sec). This extends to the Sicily channel. This area has been identified in gravity studies as thicker crust than the eastern part of Libya. The Ionian crust manifests itself as a low group velocity zone at periods above 40 sec for Rayleigh waves. This low group velocity zone also appears on the Love map at periods of 40 sec.

This study is different in that it is a smaller scale compared to previous studies and it covers the northern part of Libya using data recorded at the Libyan Network for the first time. This study delineated some changes in crustal thickness in northern Libya as well as highlighting the lithospheric structure in the central Mediterranean. We believe this study has identified some geological features in the area. However, more investigation is needed to resolve the continental features of northern Libya, which this study did not cover due to lack of data.

1.6 CONCLUSION:

We performed a tomographic inversion of group velocities for Love and Rayleigh waves over periods of 20-80 sec on a grid of 2.0° x 2.0° utilizing new data retrieved from the Libyan Seismic network. The crustal transition of the continental-oceanic crust was mapped off shore of the Libyan coast and in the central Mediterranean. The variation suggests a thin oceanic crust (<15 km) in the Ionian Sea. There is a gradient in thickness from the margins of offshore Libya towards the central Mediterranean. The continental region shows a reduced group velocity of 2.8-3.0 km/sec and the oceanic crust a group velocity above 3.2 km/sec for Rayleigh waves with periods of 28-35 sec and Love waves with 37 and 40 sec periods. There is a change in thickness (12-15 km) that extends from the Sicily channel towards the Ionian Sea that matches the results of previous gravity studies. The group velocity of the Abyssal plain and the Ionian Sea were successfully delineated in the short period of Rayleigh wave data. The Ionian Sea showed a very thin oceanic crust (12-15 km) compared to the Malta Escarpment and the Calabrian accretionary prism. The Hellenic Subduction Zone is characterized as low group velocity 2.7-3.0 km/sec zone compared to the Calabrian subduction zone (2.8 to 3.0 km/sec).

CHAPTER 2: STRESS FIELD ORIENTATIONS FROM INVERSION OF EARTHQUAKE FOCAL MECHANISMS

2.1 INTRODUCTION:

Libya is located on the Mediterranean foreland within the African platform and includes several large intra-cratonic basins. These basins have been tectonically active during the late Tertiary and Holocene (Goudarzi 1980). The early tectonics of Libya was controlled by the evolution of Gondwana and Pangaea during the Paleozoic and early Mesozoic. The development of the Mediterranean has been the main factor controlling the tectonics of Libya within the late Mesozoic and Cenozoic. Studies of plate tectonics for Africa-Europe motion predict a velocity of 7.0 ± 1.9 mm/yr1 in the direction of (N16° ±20°W) (Ward 1994). Studies have shown that the development of the Sirt intra-cratonic basin, the major feature of central Libya, and the other marginal basins (fig. 2.01) is related to two sets of movements, inter-plate motion between Africa and Europe as well as intra-plate motion within the African plate.

The Sirt Basin was formed as a response to the extensional collapse of the Sirt Arch (Van der Meer and Cloetingh 1993). Seismic activity is mostly observed in the NW part of Libya (Al-Heety 2006). The highest seismic activity is concentrated along the eastern side of the Hun Graben (Kebeasy 1980). The Hun Graben represents the NW boundary of the Sirt Basin. It is one of a series of NW-SE striking grabens, horsts, troughs and platforms that define the Sirt Basin (fig. 2.01). It extends 250 km in length and is 40-60 km wide. The northern part of the graben is characterized by relatively high seismicity. This high seismicity has been attributed to tectonic mechanisms rather than the increase of earthquake monitoring (Al-Heety 2011). Previous studies of fault plane solutions indicate that the maximum compressive stress in NW Libya is in a WNW direction, while in NE Libya the stress direction is oriented NE-SW (Al-Heety 2011). Waveform

modeling studies show strike – slip mechanisms with focal depths between 15 and 21 km (Suleiman and Doser, 1995).

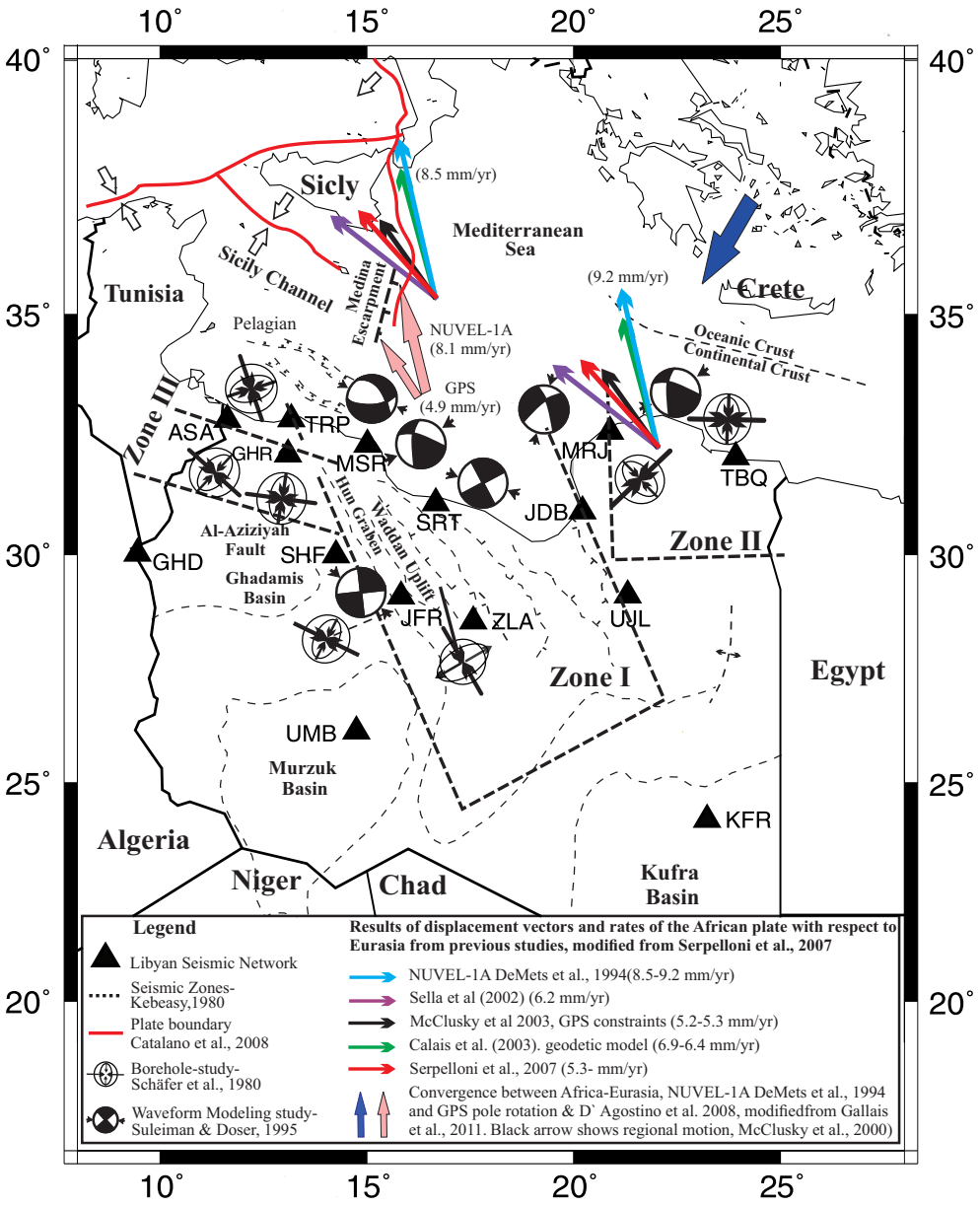

Figure 2.01: Location map and structure elements in Libya as well as results of previous studies of focal mechanisms.

Kebeasy (1980) suggested that the region can be divided into three seismic zones where Zone I includes the region of the Gulf of Sirt, Zone II includes the area of the northeastern Libya

(Cyrenaica), and Zone III covers the Al Aziziyah fault zone, which extends from the western Libyan boundary to the Hun Graben (fig. 2.01).

2.1.1 Deformation in the Libyan region:

The deformation in northern Libya has been studied by Kebeasy (1978), Westaway (1990), Al-Heety (2006; 2011). These studies were based on regional or teleseismic waveform modeling or in situ stress measurements. These studies indicate that in the northeastern part of the country (Cyrenaica) earthquake focal mechanisms show P-axes are oriented in a NE direction and associated with thrust faulting. The western part of Cyrenaica appears to be subjected to NE-SW compression (Schafer et al., 1980). In the northwestern part of Libya (Tripolitania) strike slip faulting is common (Capitanio et al., 2011) with maximum horizontal stress oriented NW-SE and normal to the direction of minimum stress. The estimated maximum horizontal stress direction across the southern Hun Graben is also oriented northwest southeast. Absolute values of stress from borehole studies are estimated to be in range of 50-150 bars (Schafer et al., 1980). On the eastern side of the country the stress is estimated to be around 0-50 bars (Schafer et al., 1980). This suggests that the northern graben is dominated by extension and the central graben is undergoing strike-slip deformation. Our goal in this study is to invert for regional stress orientations from the focal mechanisms of smaller magnitude events to determine if these regional stress orientations are observed at a more local level.

This study is different from the previous studies in that it also utilizes relatively new data from the Libyan national seismic network (LNSN). We believe that by using this new data, it will allow us to better constrain focal mechanism solutions compared to previous studies that had to rely on data from seismic networks operating outside of Libya as well as waveform modeling. Understanding stress distribution in Libya is of great importance to oil exploration since fluid

migration and accumulation are controlled by rock stresses. In addition, understanding the stress field and complex deformation of northern Libya within the context of plate tectonics is important. The kinematic deformation related to faults in the Libyan region is not fully understood in terms of African-Eurasian collision. Although deformation is expected near or along plate margins, there is no good explanation for the strain field in the interior continents far from converging plates (Capitanio et al., 2011).

2.1.2 Deformation in the central Mediterranean (plate tectonic review):

One of the main primary controls of the deformation in the central Mediterranean is the ongoing convergence between Africa-Eurasia, which has a rate of 6mm/yr in the NNW direction near Greece. The range changes to 5-7 mm/yr in the NW direction close to Sicily (Gallais et al., 2011) (fig. 2.01). According to Viti et al. (2011) the motion of the Africa relative to Eurasia is also NNW. However, the deformation in northwestern Libya still remains unresolved in the context of the deformation in the central Mediterranean.

2.2 DATA:

We collected waveform data for 10 local earthquakes that occurred within the Libyan region between 2008 and 2010 (table 2.1) recorded by the Libyan National Seismological Network (LNSN). The data were received in SEISAN format and processed in the same format. The response files for the stations were provided in SEISAN format as well. In addition to these local events obtained from the Libyan network, we collected fault plane solutions from other sources and previous studies including the International Seismological Center ISC (table 2.2). The previous fault plane solutions are mainly from waveform modeling or from stations that are located outside Libya (table 2.2). We selected events with shallow depths (0-35 km) and located south of 34 N latitude. In this way we eliminated events possibly associated with subduction.

Table 2.1: Results of the local earthquake relocations and focal mechanisms

No.	Time	Long.	Lat.	Strike	Dip	Rake	Dep. (Km)	Mag. (mb)
1	2008-01-20-20:46:48.8	10.705	33.418	77	49	-145	0.0	4.1
2	2008-05-31-02:05:43.7	19.528	32.045	134	72	159	0.0	3.4
3	2008-07-01-14:42:24.5	14.226	33.183	296	14	-89	0.1	2.5
4	2009-03-08-20:15:10.3	16.339	31.587	90	65	-8	0.1	4.2
5	2009-04-25-23:41:39.5	15.181	30.700	330	90	42	0.0	3.9
6	2009-09-27-16:56:02.8	14.262	33.025	225	54	59	0.1	4.2
7	2009-09-27-19:37:02.2	14.383	33.048	103	48	41	0.0	3.9
8	2009-12-29-11:08:51.6	15.234	32.881	349	39	-62	0.1	5.5
9	2010-05-30-19:38:33.6	16.346	31.479	4	47	-68	0.0	3.9
10	2010-08-29-14:54:12.3	15.269	32.888	10	58	-47	0.0	4.6

Table 2.2: Focal Mechanisms obtained from the (ISC, Suleiman and Doser, 1995).

No.	Time	Long.	Lat.	Strike	Dip	Rake	Dep. (Km)	Mag. (mB, MW)	Focal Mec. Solution determination Method	Source
11	1982-8-17-22:29.80	22.90	33.70	36	57	88	23.4	5.8	Regional waveform (Stations outside Libya)	ISC
12	1887-6-28-50:20:50	24.49	32.55	62	85	-130	15	5.3	Regional waveform (Stations outside Libya)	ISC
13	1988-01-28-48:13:01	21.01	32.41	158	80	-16	15	5.2	Regional waveform (Stations outside Libya)	ISC
14	1988-03-26-07:36:04	13.29	33.41	176	61	-5	15	5.1	Regional waveform (Stations outside Libya)	ISC
15	1990-11-11-11:57:39	12.28	33.73	21	90	0	15	5.2	Regional waveform (Stations outside Libya)	ISC
16	1999-02-10-05:51:50	15.01	32.93	75	88	179	34.7	5.2	Regional waveform (Stations outside Libya)	ISC
17	2002-07-16-06:56:25	24.57	33.57	179	72	-14	30.3	4.6	Regional waveform (Stations outside Libya)	ISC
18	2009-09-29-08:56:03	15.04	32.56	103	60	-74	15	5.0	Regional waveform (Stations outside Libya)	ISC
19	2012-07-03-03:40:07	14.71	33.91	140	80	-5	13.6	4.8	Regional waveform (Stations outside Libya)	ISC
20	1935 M1	15.20	31.00	349	89	2	21	7.1	Waveform Modeling	Suleiman and Doser, 1995
21	1935 A1	15.46	30.92	348	92	2	15	6.0	Waveform Modeling	Suleiman and Doser, 1995
22	1935 A2	15.56	30.93	350	89	4	19	6.5	Waveform Modeling	Suleiman and Doser, 1995
23	1963	20.00	33.18	327	62	-149	----	4.6	First motion data	Suleiman and Doser, 1995
24	1963b	21.18	33.50	139	65	-91	----	4.4	First motion data	Suleiman and Doser, 1995
25	1967	23.00	33.19	176	56	134	----	4.6	First motion data	Suleiman and Doser, 1995
26	1972	15.85	31.70	189	72	125	----	5.5	First motion data	Suleiman and Doser, 1995

2.3 METHODS:

We used the HYP software, which is implemented in SEISAN (Ottemoller et al., 2013), to locate the local events. We implemented a new velocity model (table 2.3) based on previous studies of crustal thickness in the area by Brown (2004). The LNSN velocity model has very low velocities (6.15 km/sec) at lower crustal depths, overlying a fast (8 km/sec) upper mantle that is not consistent with density models for the region. First motions arrival times, polarity, and amplitudes were picked manually using SEISAN. The focal mechanisms solutions for the given data were calculated using FOCMEC, FTPIT, PINV, and HASH. These codes are implemented in SEISAN software (Ottemoller et al., 2013). The results of the focal mechanisms obtained for these four methods were then compared to each other to determine the error in the solutions. The standard deviation is calculated for the four solutions. The final focal mechanism solution was based on the best solution determined by any of the above-mentioned codes (see the appendix for more details about the calculated focal mechanisms). We then used the stress inversion program of Vavryčuk (2014) to determine the stress direction from the first motions (Matlab code). This method is a modification of Michael's method (1984). This method relies on applying instability constraints when identifying the fault plane from the two nodal planes. Vavryčuk argues that the joint inversion for stress and fault orientation can provide a robust solution.

Table 2.3: The Velocity model used in the study.

The LNSN Velocity Model		New Velocity Model	
Velocity (km)	Depth (km)	Velocity (km)	Depth (km)
3.24	00.0	5.45	00.0
4.80	04.0	5.53	03.0
5.60	08.0	6.20	10.0
5.80	14.0	6.40	20.0
6.15	23.0	7.16	30.0
8.00	32.0	7.50	35.0
8.25	50.0	7.65	40.0
8.50	80.0	7.85	50.0

2.4 RESULTS:

2.4.1 Focal mechanisms:

The 10 focal mechanisms are given in (Table 2.1) and shown in (fig. 2.02). The located events are distributed along the Libyan shore and have a magnitude range of 2.5 to 5.5 m_b. In the NE part of Cyrenaica the focal mechanism indicates an oblique reverse fault (mechanism number 2 on the map of (fig. 2.02). In the northwestern part of the Libyan region the results show mainly mix of normal and reverse (fig. 2.02) faulting. The other focal mechanism results show both oblique normal faults as well as strike slip faults. We implemented a classification to show the degree of certainty of the solutions (table 2.4). We calculated the standard deviation of all four solutions. The assigned weight or classification given to each solution is in the range of A, B and C, where A is well determined and C is acceptable (table 2.4).

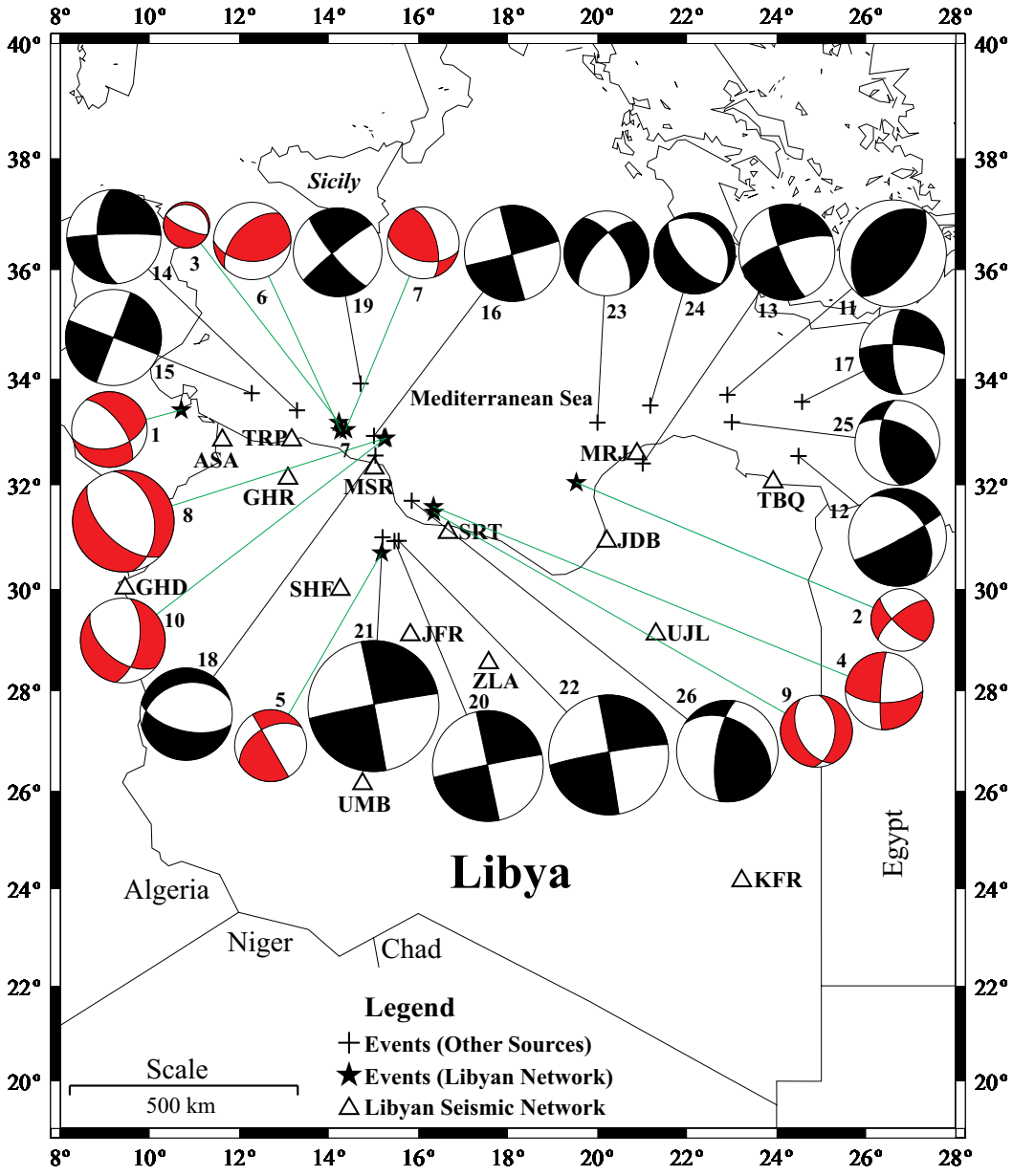

Figure 2.02: Results of the focal mechanisms obtained in this study in addition to other data collected from other sources. The numbers shown are the event numbers given in table 2.3 and 2.4. the size of the focal mechanism relates to magnitude. the focal mechanisms from this study are highlighted in red.

Table 2.4: Classification of the focal mechanisms results obtained in this study.

No.	STANDARD DEVIATION OF THE FOCAL MECHANISM RESULTS (FOCMEC, FTPIT, PINV, & HASH)			Arbitrary confidence of the fault plane solutions (A=well defined, B=good, C=acceptable)	Number of Stations used
	STRIKE	DIP	RAKE		
1	123.00	06.50	48.50	C	5
2	042.00	06.00	80.50	B	5
3	098.00	25.50	09.50	C	3
4	046.59	11.67	61.07	A	7
5	153.00	14.61	91.45	C	9
6	056.00	00.50	47.00	B	6
7	043.27	02.49	35.14	A	7
8	018.37	09.74	02.45	A	9
9	005.50	01.50	03.00	A	7
10	068.13	11.56	30.00	A	9

2.4.2 Inversion results:

To determine stress orientation we separated the study region into 3 different areas as suggested in previous studies. The NE area which represents zone II consists of 8 focal mechanisms. Zone I is around the Sirt Basin and contains 7 focal mechanisms. Zone III, which is in the NW, has 11 focal mechanisms (fig. 2.01). We did this based on the fact that we are presumably dealing with at least two different stress regimes. In addition, the located earthquakes appeared to separate into 3 distinct regions within Libya. The dominant focal mechanisms in Zone I vary from strike slip faults to oblique normal faults. The inversion results show that (σ_1) has a strike of 95° and a plunge of 22° (table 2.5). Zone II, near to the Hellenic subduction zone, shows oblique normal to strike slip faulting and one thrust fault. The inversion results show that the maximum stress (σ_1) has a strike of 327° and plunge of 13° (table 2.5) and (fig.2.05). The focal mechanisms zone III show oblique normal and strike slip faults. The maximum stress (σ_1) strikes 129° and plunges 16°. The output results of the code are shown in (fig. 2.03 and 2.04). See the caption figures for details.

Table 2.5: Summary of the focal mechanism inversion results.

Zones	Focal Mechanism used in the inversion	σ_1 Azimuth/Plunge	σ_2 Azimuth/Plunge	σ_3 Azimuth/Plunge	Shape Ratio
Zone I (Middle)	7	95 /22	305 /64	189 /11	0.50
Zone II (Eastern)	8	327 /13	82 /60	230 /25	0.84
Zone III (Western)	11	129 /16	342 /70	222/ 09	0.73

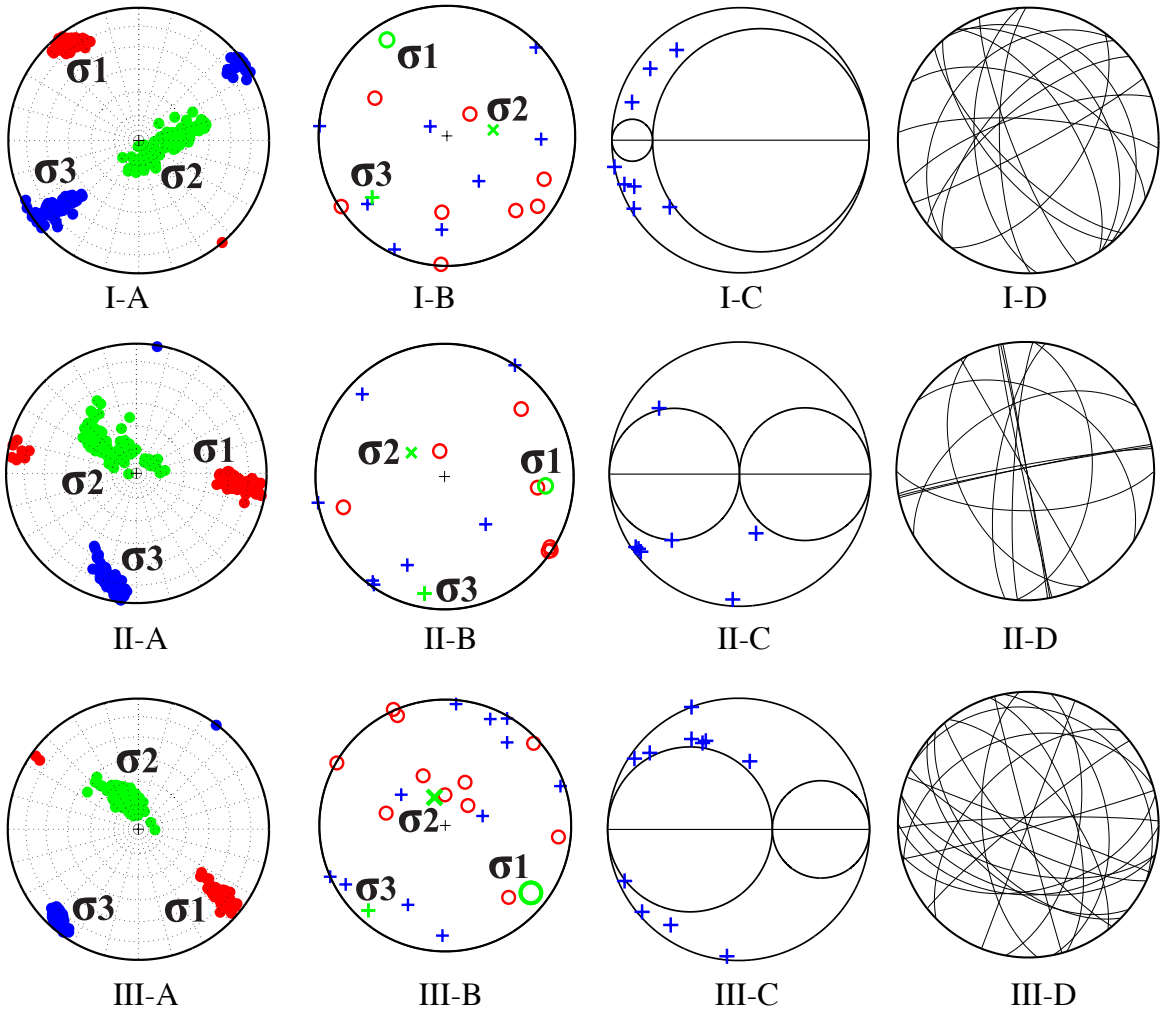

Figure 2.03: Results of the focal mechanism inversion for zones I, II, & III. Figures I-A, II-A, & III-A show the confidence region limits for the principles stress directions for the three zones. Figures I-B, II-B, & III-B show the P/T axes with the retrieved principle stress. Figures I-C, II-C, & III-C show the Moher circle representation for the stress. Figures I-D, II-D, & III-D show the corrected fault plane solutions after the inversion.

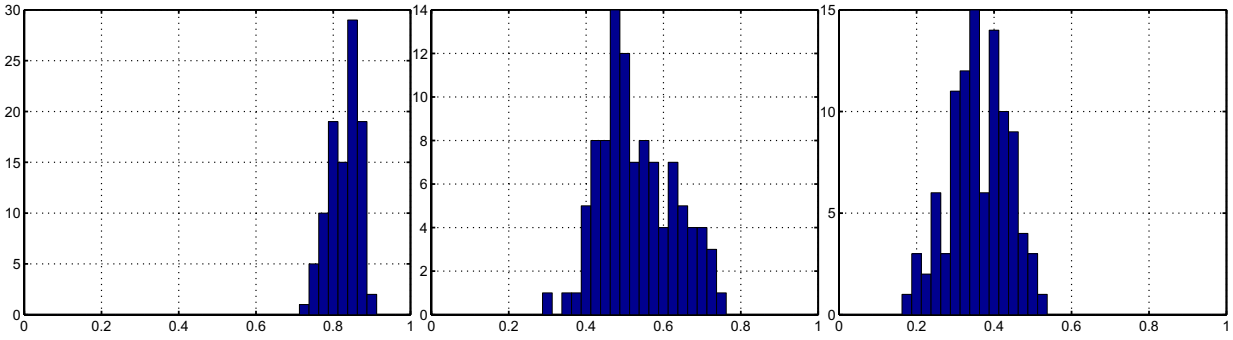

Figure 2.04: Shows part of the inversion results for the zones I, II, & III. The figures (I-E, II-F, & III-G) show the relative magnitude of principles stress represented a shape ratio (r= σ2 – σ1/ σ3 – σ1). The r ratio is considered acceptable if it falls between 0.75 and 0.82 Bellier and Zoback 1995.

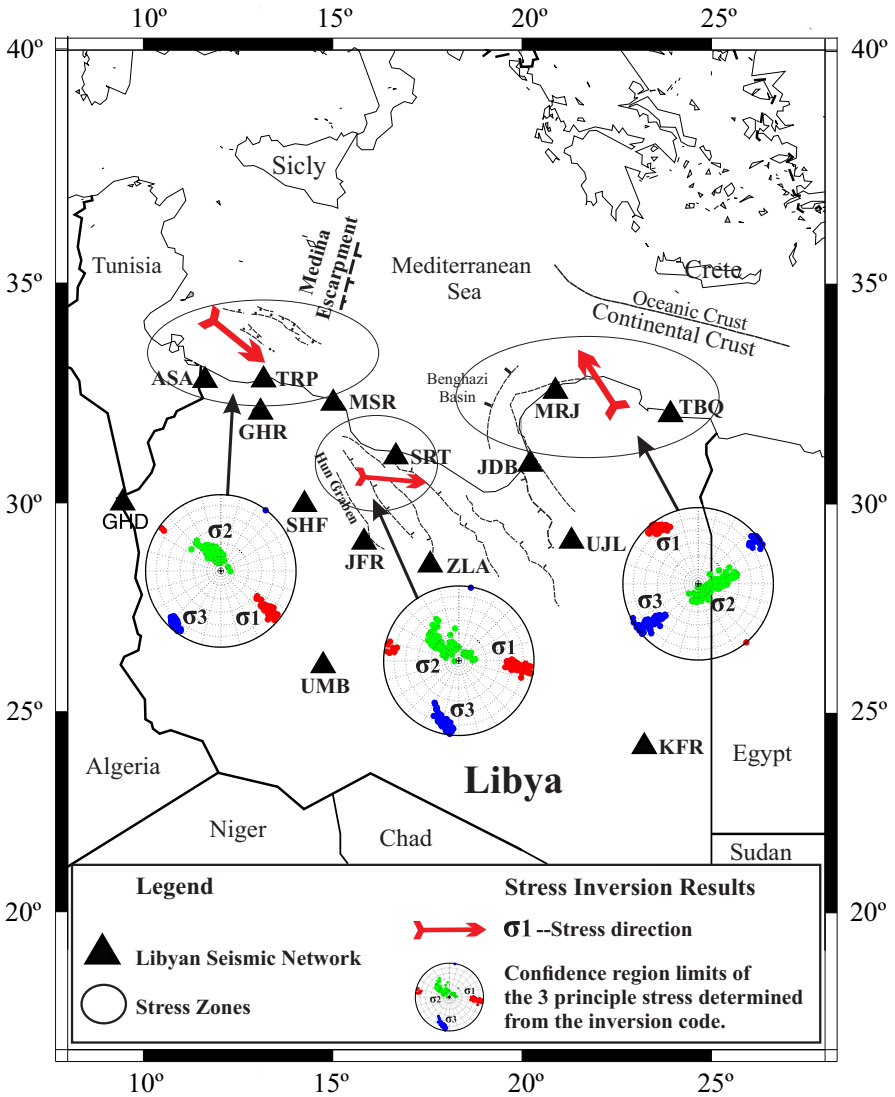

Figure 2.05: Location map showing the results of the stress inversion. The red arrows show the change in the main stress direction.

2.5 DISCUSSION:

We conducted a stress inversion using a new Matlab code developed by Vavryčuk (2014). The study area was divided into three different seismic zones as suggested in previous studies (fig. 2.01). We provided a classification of our fault plane solutions results (for more details about the focal mechanism solutions see the Appendix). The stress inversion results show consistency between the results of this study and previous analyses of stress. Although our data are very limited and below the desirable number of data needed to carry out a reliable inversion process (at least 20 focal mechanism solutions, Vavryčuk, personal communication, 2014), the results seem to be reasonable. In addition, the corrected fault plane solutions are not well determined. Generally, the focal mechanism solutions show strike slip and oblique normal faults. Previous studies tend to connect the deformation system with the complex Mediterranean stress regime as was suggested by Capitanio et al. (2009) that the Africa-Eurasia relative motion is in the S-SW to N-NE direction.

2.6 CONCLUSION:

We presented a total of 10 new focal mechanisms solutions for events recorded by the Libyan seismic network. A new velocity model for the Libyan area was suggested in this study. We inverted for the stress field in the region using the new focal mechanisms and results from previous studies. At least two different stress regimes were determined, comparable to previous studies. In Cyrenaica (zone II) the stress field shows maximum principal stress oriented perpendicular to the Hellenic subduction zone. In Northwestern Libya (zone III) the maximum principal stress is directed towards southeast. In north-central Libya (zone I) the maximum principal stress is in the east-southeast direction. The results suggest that zones I and III have similar stresses, but that maximum compressive stress in zone II is in the same direction as GPS motion vectors for the interaction of the African and Eurasia plates. Zones I and III show maximum compressive stress that is at an angle to plate convergence.

CHAPTER 3: CRUSTAL THICKNESS FROM RECEIVER FUNCTION BENEATH LIBYA

3.1 INTRODUCTION:

The development of the Mediterranean and Tethys oceans had a primary effect on the tectonics of Libya during the late Mesozoic and Cainozoic. Earlier tectonic development of Libya was controlled by the evolution of Gondwana and Pangaea within the Paleozoic and Mesozoic. In addition, inter-plate tensions have significantly affected the tectonics in Libya (fig.3.01). The crustal thickness (Moho depth) and velocity in the Libyan region is poorly understood (e.g., Sandvol et al., 1998; Van der Meijde et al., 2003 and 2005; Marone et al., 2004; Pasyanos and Nyblade 2007; Pasyanos 2010; Roure 2012). This is due to sparse observations, lack of data, and inhomogeneous coverage of seismograph stations within the region. On the eastern side of the Libyan margin there is also depth uncertainty of the African continental part (Casten et al., 2006). Prior to this study, only one receiver function (RF) analysis of the region had been conducted.

Van der Meijde et al. (2003) investigated the crustal thickness at twelve broadband seismic stations in North Africa, including two Libyan stations GHAR (GHR) and MARJ (MRJ). This analysis was based on a new grid search method for estimating crustal thickness and obtained an estimate of 30 ± 2.1 km at GHR (GHAR) and 31 ± 1.5 km beneath MRJ (MARJ). In addition, the estimated crustal thickness at the Eurasian-African plate boundary (Mediterranean) was 45 km. Van Der Meijde et a. (2005) studied the deeper velocity discontinuities in the Mediterranean area concentrating on the upper and lower mantle. They reported velocity discontinuities of 413 and 634 km and 420 and 684 km under GHAR and MARJ, respectively.

However, these depths have larger uncertainties of ±18 km. The velocity model they used in this study was the EAV03 model of the Mediterranean.

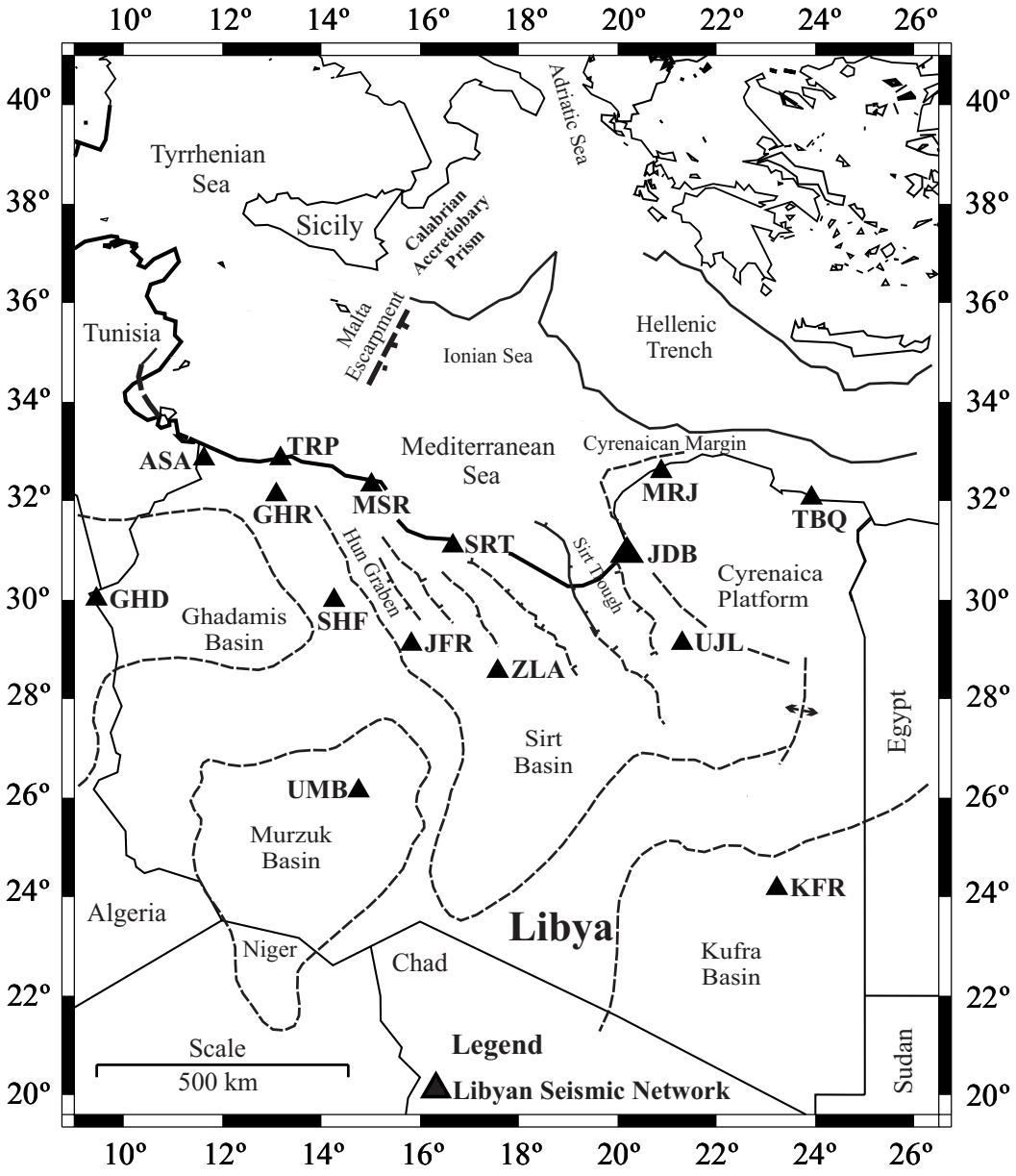

Figure 3.01: Location map shows the main geological and structural elements modified from Abadi et al. (2008).

An upper mantle transition zone (260-275 km) was observed in North Africa under MARJ, which is consistent with the observed velocity anomaly (EAV03) in eastern Libya. Crustal thinning has been suggested in northern Libya, especially beneath the rifted areas within the Sirt basin. This has been interpreted from the increase of regional gravity from south to north within the Sirte Basin (Suleiman and Doser, 1995).

3.1.1 Gravity studies:

Tedla et al. (2011) developed a large-scale crustal model for Africa using free-air anomaly gravity data. The crustal thickness was estimated using 3-D Euler deconvolution. Their results have shown that the average crustal thickness for the whole continent is 39 ± 2 km. The crustal thickness of the offshore Libya particularly in the Sirt basin shows a thinner continental crustal thickness less than 15 km (Tedla et al., 2011).

3.2 DATA:

We obtained a total of 67 teleseismic events recorded from 2005-2010 at the Libyan National Seismological Network Stations (LNSN). The data were recorded on a 3 component of broadband stations that cover most of the Northern part of Libya (fig. 3.01). The data were received from the LNSN in SEISAN format. The data preparation included conversion from SEISAN to SAC format in order to estimate the RF. All events that we attempted to analyze are given in (table 3.1). Note that most of these events could not be used because of the poor signal to noise ratios of the seismograms. In the best cases there were about 20 events left per station after processing the data.

Table 3.1: Teleseismic events used to calculate the receiver functions.

No	EVENT ID	SOURCE	DATE	TIME	LAT.	LON.	DEPTH	MAG.
01	8730181	ISC	2005-06-02	11:04:53.90	033.93	135.19	008.0	0.1
02	8909974	ISC	2005-07-23	07:47:45.00	042.29	139.34	016.0	1.3
03	8910147	ISC	2005-07-23	14:45:11.20	035.61	140.11	063.0	0.7
04	8527713	ISC	2005-07-26	14:22:03.80	016.72	-099.64	005.8	3.6
05	8111428	ISC	2005-08-22	01:31:38.09	036.07	025.46	107.4	3.8
06	9040599	ISC	2005-09-09	07:43:51.90	035.46	136.48	016.0	0.8
07	7704458	ISC	2005-10-23	10:20:44.62	-040.57	175.71	041.9	3.8
08	7758935	ISC	2005-11-17	19:38:03.00	062.04	002.48	000.0	2.2
09	9068963	ISC	2005-11-21	15:48:27.90	033.62	130.40	008.0	0.3
10	9123226	ISC	2005-12-12	21:13:30.50	043.27	139.39	037.0	1.7
11	9126039	ISC	2005-12-23	22:00:58.50	039.05	140.94	007.0	1.7
12	10597742	ISC	2006-03-05	08:27:10.90	036.66	141.31	040.0	1.6
13	10412440	ISC	2006-04-17	02:41:54.80	025.01	036.09	015.0	1.8
14	9801503	ISC	2006-05-04	02:27:25.30	036.70	141.20	047.0	1.1
15	10628960	ISC	2006-05-13	03:21:03.90	044.12	044.41	014.0	3.8
16	8713723	ISC	2006-05-19	14:55:36.03	002.16	126.95	047.6	4.4
17	9807608	ISC	2006-05-22	13:20:51.60	033.80	134.32	013.0	0.3
18	8463549	ISC	2006-05-28	03:23:56.22	042.17	073.64	010.0	3.0
19	9812048	ISC	2006-06-02	07:49:04.90	043.87	148.34	000.0	3.9
20	9818669	ISC	2006-06-22	11:04:59.30	041.89	142.18	034.0	1.4
21	9820272	ISC	2006-06-27	03:21:43.90	035.42	139.01	024.0	0.4
22	9601119	ISC	2006-07-17	08:29:15.42	-009.32	107.16	000.0	4.5
23	9991467	ISC	2006-08-11	21:00:36.20	042.42	141.90	101.0	2.3
24	9992044	ISC	2006-08-13	10:34:56.50	036.11	140.01	063.0	0.4
25	9672614	ISC	2006-08-17	15:32:02.12	-002.65	-078.37	012.0	4.0
26	9994181	ISC	2006-08-20	03:49:17.40	023.36	122.22	026.0	2.9
27	10081888	ISC	2006-09-11	18:21:01.70	035.75	136.85	009.0	0.3
28	10118674	ISC	2006-11-24	17:22:46.30	025.06	123.62	018.0	1.6
29	10466402	ISC	2006-12-09	15:00:12.10	037.41	138.90	012.0	0.3
30	11500463	ISC	2007-02-11	06:20:34.83	019.31	-064.23	025.3	3.0
31	11921505	ISC	2007-04-10	10:40:29:00	024.70	122.77	097.0	3.2
32	11934182	ISC	2007-04-25	13:48:22.27	053.10	-169.55	152.7	2.9
33	11935471	ISC	2007-04-27	08:10:57.60	037.33	136.71	004.0	1.5
34	12775408	ISC	2007-07-21	15:42:24.90	039.55	142.10	087.0	3.0
35	12817265	ISC	2007-08-31	20:51:01:00	038.55	-029.14	000.1	3.0
36	12962182	ISC	2007-09-12	11:19:57.90	060.72	028.97	000.0	1.1
37	12964236	ISC	2007-09-14	06:12:58.08	036.99	-005.37	011.5	1.6
38	601075007	ISC	2007-09-23	00:53:44:00	-039.30	177.89	025.8	2.9
39	12972151	ISC	2007-09-26	18:44:49.90	040.04	038.96	008.0	2.7
40	13233819	ISC	2007-10-02	18:13:03.20	041.73	142.49	050.0	1.5
41	13270655	ISC	2007-11-20	18:04:42.30	031.89	131.02	012.0	0.6
42	13273652	ISC	2007-11-25	03:00:41.60	038.07	142.10	039.0	1.4
43	13287444	ISC	2007-12-11	16:01:37.06	035.03	077.42	045.6	4.2
44	13327312	ISC	2008-01-04	07:37:19.26	039.40	033.14	007.0	2.0
45	11437736	ISC	2008-02-04	12:00:57:00	028.64	129.82	030.0	1.7

No	EVENT ID	SOURCE	DATE	TIME	LAT.	LON.	DEPTH	MAG.
46	11435475	ISC	2008-02-04	22:08:23.40	031.99	130.26	010.0	1.0
47	11439073	ISC	2008-02-19	23:14:21:00	034.71	132.33	020.0	2.1
48	13214474	ISC	2008-02-20	18:26:34:00	065.25	22.572	003.5	2.0
49	14006040	ISC	2008-04-01	10:44:44.70	038.07	048.52	005.0	2.8
50	12853764	ISC	2008-05-22	20:56:00.56	027.86	052.83	010.0	3.0
51	11636519	ISC	2008-05-23	08:40:38.20	038.88	141.59	72.00	0.3
52	13515191	ISC	2008-08-03	00:41:20:00	037.39	138.50	010.0	0.6
53	13515871	ISC	2008-08-04	19:42:47:00	040.37	139.00	012.0	1.5
54	12608730	ISC	2008-09-10	11:02:38.40	032.19	104.50	013.0	3.5
55	11348159	ISC	2008-10-04	02:08:23:00	018.91	-064.77	045.3	3.1
56	13932395	ISC	2008-10-12	19:04:38.00	-042.88	-072.56	022.8	3.3
57	13397675	ISC	2008-10-21	04:32:25.40	017.46	-094.29	194.0	3.9
58	14119954	ISC	2008-11-09	12:52:59.90	-042.85	-072.59	011.9	3.3
59	12077260	ISC	2008-12-13	08:26:37.21	-030.46	-177.07	000.0	3.8
60	12081030	ISC	2009-01-11	12:31:25.06	-001.03	132.88	000.0	3.5
61	14358698	ISC	2009-02-01	00:54:39.14	040.96	043.31	011.9	3.1
62	15467871	ISC	2009-08-21	13:41:09:00	042.86	145.54	043.0	2.3
63	15412286	ISC	2009-04-09	19:36:26:00	036.35	141.36	046.0	1.6
64	15743973	ISC	2009-09-06	21:46:26:00	030.12	050.67	033.5	2.2
65	15499450	ISC	2009-11-03	05:26:10:00	031.19	132.51	049.0	2.3
66	14308214	ISC	2009-11-11	09:53:15:00	039.15	069.97	103.0	4.1

3.3 METHODS:

We used teleseismic P waveforms recorded at three component stations of the LNSN. Calculating receiver function relies on the fact that the P-wave signals from teleseismic earthquakes convert to S waves at Moho interface (Langston 1977; Owens et al., 1984; Ammon et al., 1990; Cassidy and Ellis, 1993; Zandt, and Ammon 1995). The Moho can then be estimated using the difference in time from the incident direct P and converted Ps. The converted phase provides information about crustal thickness and the seismic velocity of the Moho. This phase can be better identified on the radial component of seismograms. In order to improve identification of the Ps phase the radial seismogram (obtained by rotation of the horizontal components) is usually deconvolved from the vertical component to obtain the RF. This process removes the effects of the instrument response, and source and path effects (from source to base of the crust). The receiver function is computed using the frequency - domain method (Di Bona

1998) that is based on the deconvolution of the vertical components (fig. 3.02). In this method, we employed the iterative deconvolution method (Ligorria and Ammon 1999). This method minimizes the difference between the observed horizontal component seismogram and the predicted receiver function. The receiver functions were computed using Gaussian width factors of 1.0, 1.75, and 2.5.

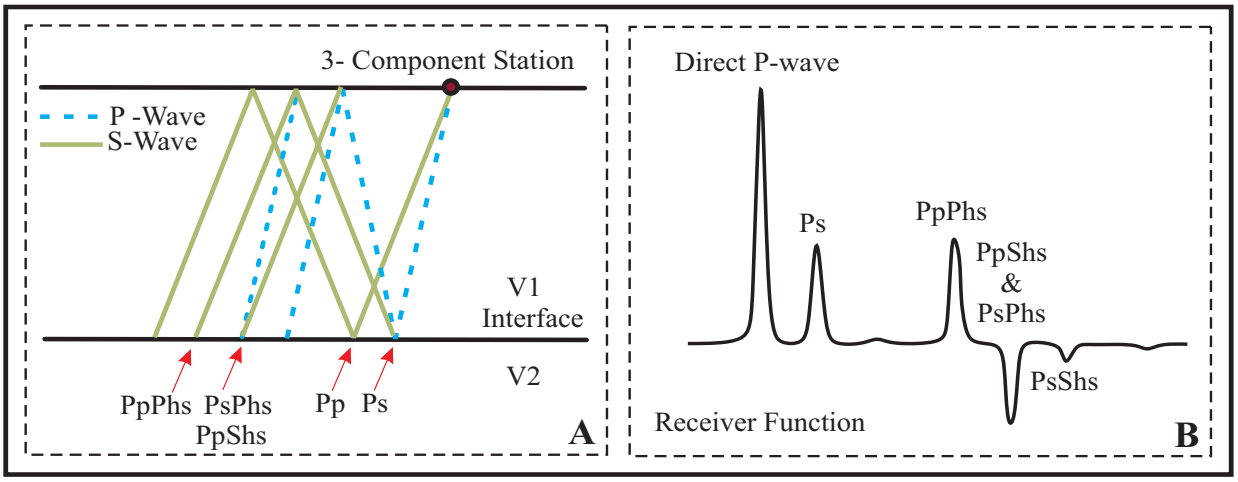

Figure 3.02: A - P to S converted waves that reverberate as a result of the local structure B - a typical receiver function (time series computed from seismograms). A typical receiver function carries the signature of the local reverbnation of the underlying geology.

3.4 RESULTS:

We computed the receiver functions for the selected teleseismic events (see the appendix). Table 3.2 shows the number of raw events as well as the final computed number of the receiver functions. The receiver functions we obtained were not consistent with the typical predicted signal (fig. 3.03). The magnitudes of the first spike of our RFs were often very small and sometimes it is reversed. Unfortunately these poor results cannot be used to determine crustal thickness. More data are needed to calculate additional receiver function.

Table 3.2: Number of receiver functions obtained

No.	Station	Number of raw Events	Number of Events Used	Number of Poor Receiver functions	Number of calculated Receiver Functions
1	ASA	57	34	20	14
2	GHD	50	30	16	14
3	GHR	46	23	12	11
4	JDB	56	15	10	5
5	JFR	49	38	22	16
6	KFR	51	27	14	13
7	MRJ	56	22	14	8
8	MSR	53	12	8	4
9	SHF	49	19	14	5
10	SRT	44	13	10	3
11	TBQ	49	29	22	7
12	TRP	16	4	2	2
13	UJL	42	17	11	6
14	UMB	51	41	27	14
15	ZLA	49	31	17	14

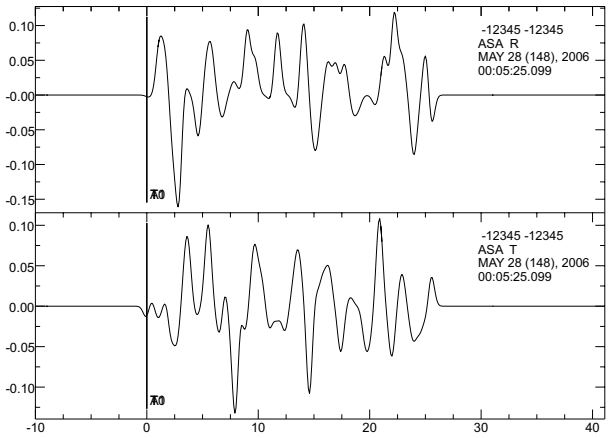

ASA station

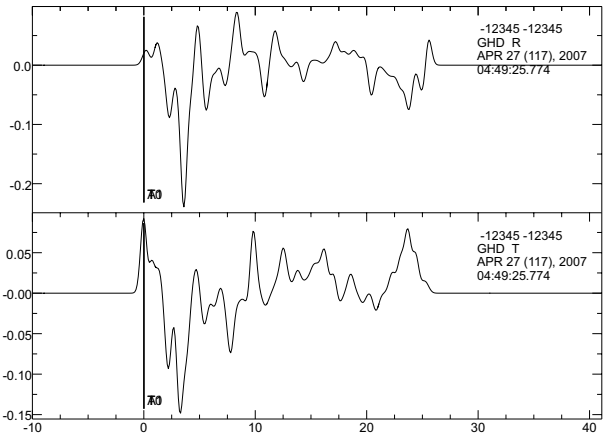

GHD station

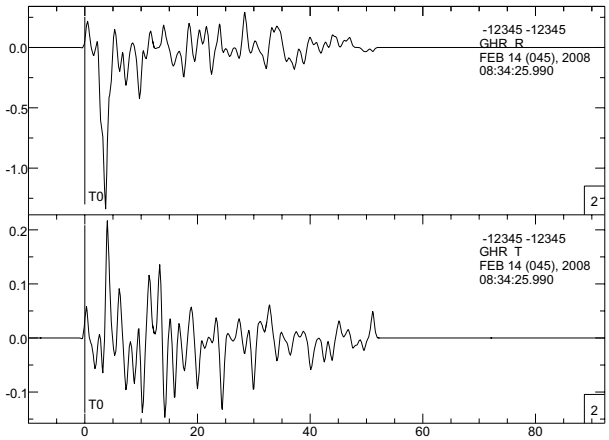

GHR station

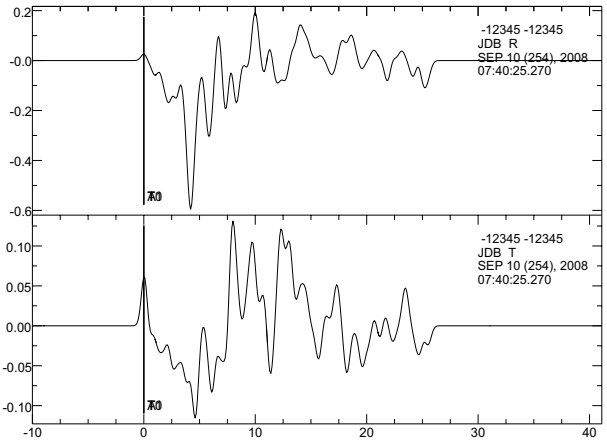

JDB station

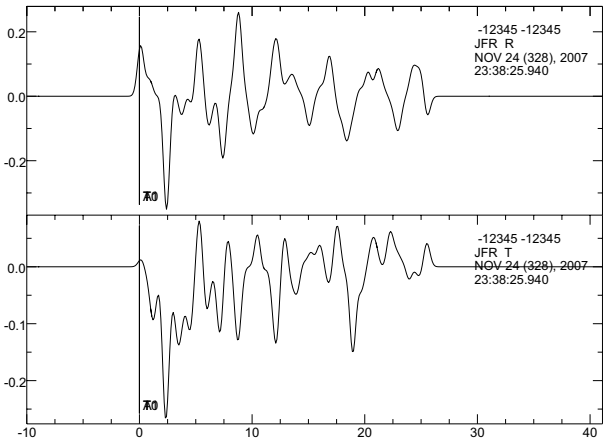

JFR station

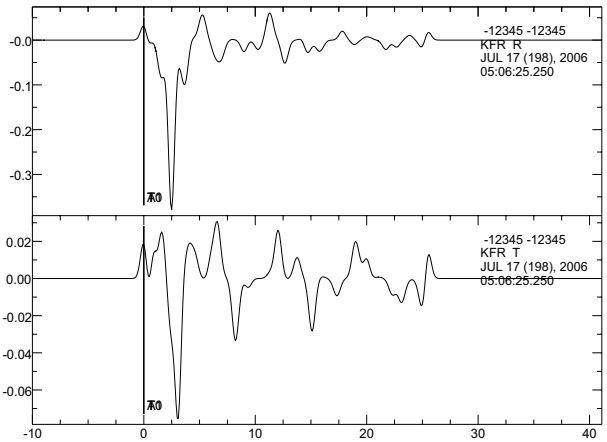

KFR station

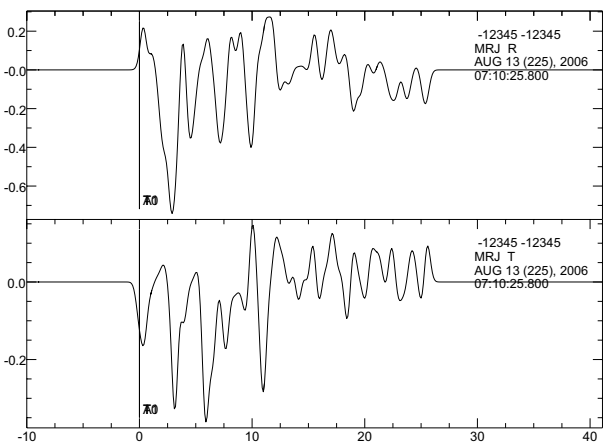

MRJ station

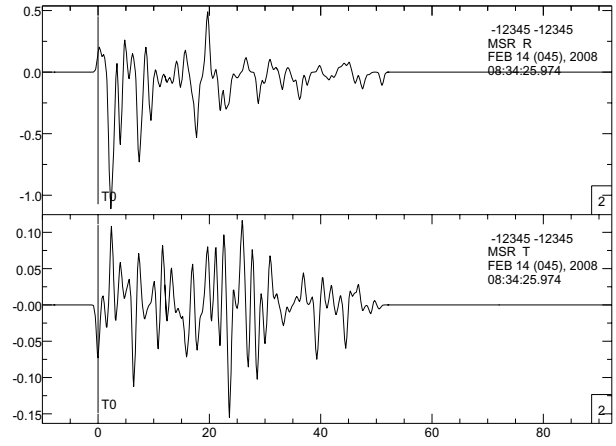

MSR station

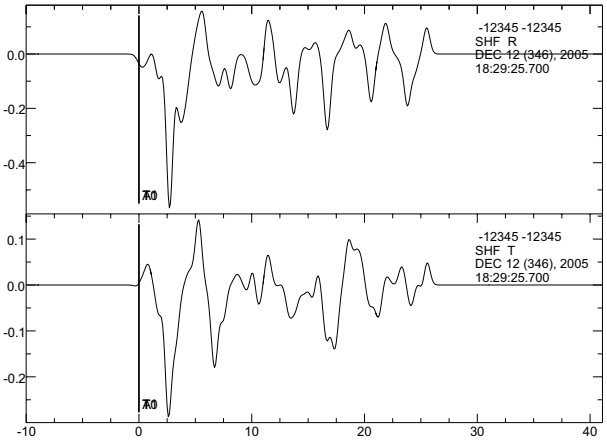

SHF station

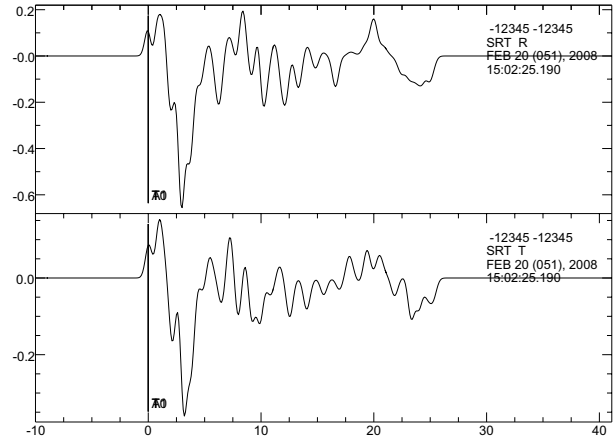

SRT station

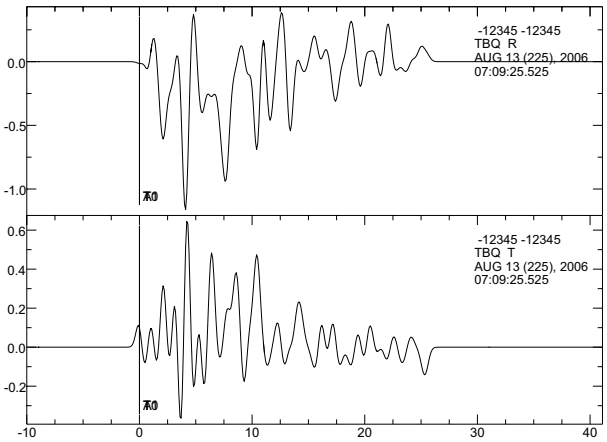

TBQ station

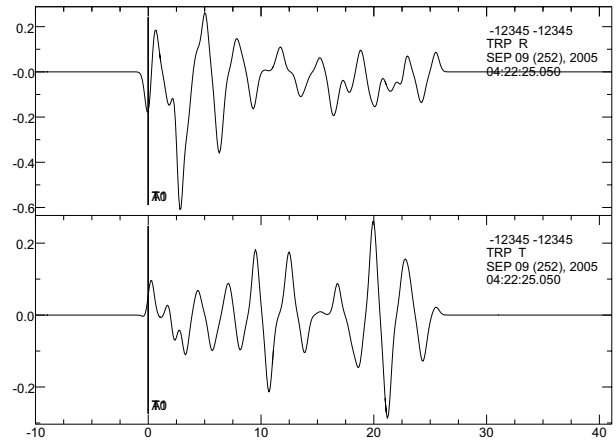

TRP station

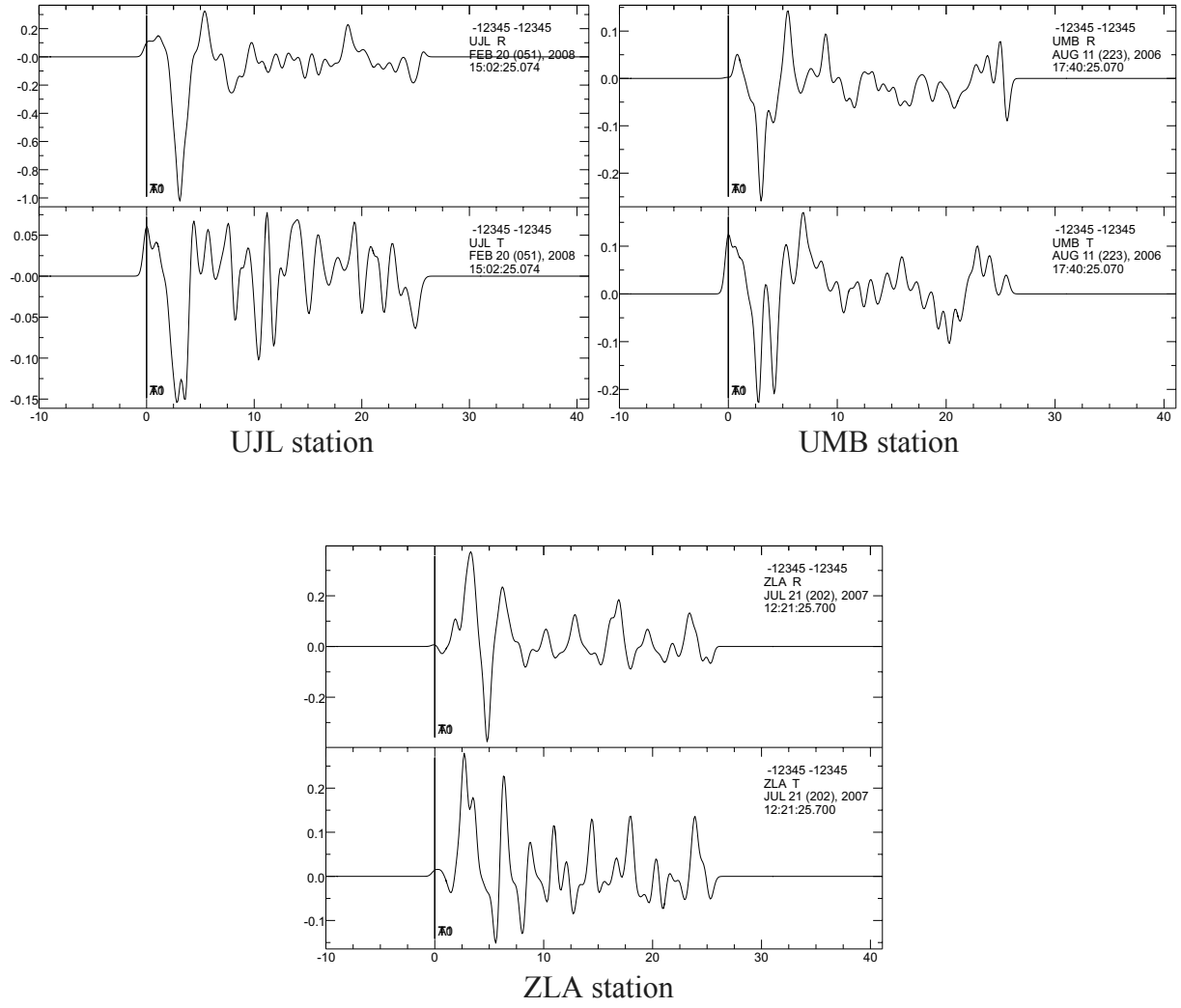

Figure 3.03: Receiver functions results for all the stations. Note the very emergent and low amplitude arrivals observed at many stations with very high amplitude reverberations. In some cases the first arrivals are even negative. These are not consistent with the shapes predicted for receiver functions (compare to fig. 3.02).

REFERENCES

Abadi, A. M., van Wees, J. D., van Dijk, P. M., and Cloetingh, S. A. P. L., 2008. Tectonics and subsidence evolution of the Sirt Basin, Libya. American Association of Petroleum Geologists Bulletin, 92, 993–1027.

Al-Heety E., and Eshwehdi A., 2006. Seismicity of the northwestern region of Libya: an example for the continental seismicity. Seismol. Res. Lett. 77(6), 691–696.

Ammon, C.J., 2001. Notes on Seismic Surface-Wave Processing, Part 1, Group Velocity Estimation Saint Louis University, version 3.9.0. http://eqseis.geosc.psu.edu/~cammon 2001

Barmin, M. P., Levshin, A. L., and Ritzwoller, M. H., 2001. A fast and reliable method for surface wave tomography. Pure Appl. Geophys., 158, 1351 – 1375.

Bellier, O., and Zoback, M.L., 1995. Recent state of stress change in the Walker–Lane Zone, Western Basin and Range Province, United States. Tectonics 14, 564–593.

Brown, Wesley, (2004), An Integrated Geophysical Study of the Lithospheric Structure beneath Libya. (Doctoral dissertation).

Boschi, L., Ekström, G., and Kustowski, B., 2004. Multiple resolution surface wave tomography: The Mediterranean basin. Geophys. J. Int., 157, 293 – 304.

Casten, U., and Snopek, K., 2006. Gravity modelling of the Hellenic subduction zone - a regional study. Tectonophysics, 417, 183-200, doi:10.1016/j.tecto.2005.11.002.

Carminati, E., and Doglioni, C., 2004. Europe - Mediterranean tectonics. In Encyclopedia of Geology, Elsevier, 135-146.

Capitanio, F.A., Faccenna, C., Funiciello, R., and Salvini, F., 2011. Recent tectonics of Tripolitania, Libya: an intraplate record of Mediterranean subduction. Geological Society of London. Special Publication 357, 319–328.

Cassidy, J. F., and Ellis, R.M., 1993. S wave velocity structure of the norther Cascadia subduction zone, J. Geophys. Res., 4407-4421.

Cowie, L and Kusznir, N.J., 2012. Mapping crustal thickness and oceanic lithosphere distribution in the Eastern Mediterranean using gravity inversion. Petroleum Geoscience, 18. pp. 373-380.

Di Bona, M., 1998. Variance estimate in frequency-domain deconvolution for teleseismic receiver function computation. Geophys. J. Int. 134, 634–646.

Doser, D. I., Crain, K. D., Baker, M. R., Kreinovich, V., and Gerstenberger, M. C., 1998. Estimating uncertainties for geophysical tomography. Reliable Computing, 4(3)241–268.

Gallais, F., Gutscher, M.-A., Graindorge, D. Chamot-Rooke, N. and Klaeschen, D., 2011. A Miocene tectonic inversion in the Ionian Sea (central Mediterranean): Evidence from multichannel seismic data. J. Geophys. Res., 116, B12108, doi:10.1029/2011JB008505.

Goudarzi, G. 1980. Structure—Libya. In: Salem M., and Busrewill M., (eds) The Geology of Libya, vol. 3. Academic Press, London, pp 879–892.

Herrmann, R. B., 1973. Some aspects of band-pass filtering of surface waves. Bull. Seism. Soc. Am, 63,663–671.

International Seismological Centre, On-line Bulletin, http://www.isc.ac.uk, Internatl. Seis. Cent., Thatcham, United Kingdom, 2013.

Kokinou, E., Vafidis, A., Loucogiannakis, M. and Louis, J., 2003. Deep seismic imaging and velocity estimation in Ionian Sea. Journal of the Balkan Geophysical Society, 6, (2), 100 - 116.

Kebeasy, R., 1980. Seismicity and seismotectonics of Libya. In: Salem, M., and Busrewill, M. (eds), Geology of Libya, vol 3. Academic Press, London, pp 955–963.

Langston, C. A., 1977.The effect of planar dipping structure on source and receiver responses for constant ray parameter. Bull. Seismol. Soc. Am., 61, 1029-1050, 1977.

Laske, G., Masters, G., Ma, Z., and Pasyanos, M., 2013. Update on CRUST1.0 - A 1-degree Global Model of Earth's Crust. Geophys. Res. Abstracts, 15, Abstract EGU2013-2658, 2013.

Ligorria, J. P., and Ammon, C. J., 1999. Iterative deconvolution and receiver-function estimation. Bull. Seism. Soc. Am. 89 1395–400

Luccio, F., and Pasyanos, M.E., 2007. Crustal and upper-mantle structure in the Eastern Mediterranean from the analysis of surface wave dispersion curves. Geophys. J. Int., 169(3), 1139–1152.

Marone, F., Van der Meijde, M., Van der Lee, S., and Giardini, D., 2003. Joint inversion of local, regional and teleseismic data for crustal thickness in the Eurasia-Africa plate boundary region. Geophys. J. Int., 154, 499 –514.

Meier, T., Dietrich, K., Stockhert, B. , and Harjes, H., 2004. One-dimensional models of shear wave velocity for the eastern Mediterranean obtained from the inversion of Rayleigh wave phase velocities and tectonic implications. Geophys. J. Int., 156, 45–58.

Martinez, M.D., Lana, X., Canas, J.A., Badal, J., and Pujades, L., 2000. Shear wave velocity tomography of the lithosphere–asthenosphere system beneath the Mediterranean area. Phys. Earth Planet. Inter. 122, 33–54.

Marone, F.,van der Lee, S., and Giardini, D., 2004. Three-dimensional upper-mantle S-velocity model for the Eurasia-Africa plate boundary region. Geophys. J. Int., 158, 109 –130.

McClusky, S., Reilinger, R., Mahmoud, S., Ben Sari, D., and Tealeb, A., 2003. GPS constraints on Africa (Nubia) and Arabia plate motions. Geophys. J. Int., 155, 126 – 138.

Michael, A.J., 1984. Determination of stress from slip data: Faults and folds. J. Geophys. Res. 89, 11.517-11.526.

Ottemoller, L., P. Voss, and J. Havskov (2013). SEISAN Earthquake Analysis Software for Windows, Solaris, Linux and MacOSX, Version 9.1,Univ. of Bergen, Bergen, Norway.

Owens, T. J., Zandt, G., and Taylor, S.R., 1984. Seismic evidence for an ancient rift beneath the Cumberland Plateau, Tennessee: A detailed analysis of broadband teleseismic P waveforms. J. Geophys. Res., 89, 7783-7795.

Pasyanos, M.E., and Walter, W.R., 2002. Crust and upper-mantle structure of North Africa, Europe and the Middle East from inversion of surface waves. Geophys. J. Int., 149, 463–481.

Pasyanos, M.E., 2005. A variable resolution surface wave dispersion study of Eurasia, North Africa, and surrounding regions. J. Geophys. Res., 110, B12301, doi:10.1029/2005JB003749.

Pasyanos, M.E., 2010. Lithospheric thickness modeled from long period surface wave dispersion, Tectonophysics, 481, 38-50, doi:10.1016/j.tecto.2009.02.023.

Pasyanos, M.E., and Nyblade, A.A., 2007. A top to bottom lithospheric study of Africa and Arabia. Tectonophysics, 444, 27-44, doi:10.1016/j.tecto.2007.07.008.

Piromallo, C., and Morelli, A., 1997. Imaging the Mediterranean upper mantle by P-wave travel time tomography. Ann. Geofis., 40(4), 963-979, 1997.

Piromallo, C., and Morelli, A., 2003. P-wave tomography of the mantle under the Alpine–Mediterranean area. J. Geophys. Res. 108, doi:10.1029/2002JB001757.

Piana Agostinetti, N., M. S. Steckler, and F. P. Lucente (2009), Imaging the subducted slab under the Calabrian Arc, Italy, from receiver function analysis, Lithosphere, 1(3), 131–138, doi:10.1130/L49.1.

Ritzwoller, M.H., and Levshin, A.L., 1998. S Surface wave tomography of Eurasia: group velocities. J. geophys. Res., 103, 4839–4878.

Rosenbaum, G., Lister, G.S., Duboz, C., 2004. The Mesozoic and Cenozoic motion of Adria (central Mediterranean): a review of constraints and limitations. Geodinamica Acta17 (2), 125–139.

Roure, F., Casero, P., and Addoum, B., 2012. Alpine inversion of the North African margin and delamination of its continental lithosphere. Tectonics, 31, TC3006, doi:10.1029/2011TC002989.

Sandvol, E., Seber, D., Calvert, A., and Barazangi, M., 1998. Grid search modeling of receiver functions: Implications for crustal structure in the Middle East and North Africa. J. Geophys. Res., 103, 26,899 – 26,917.

Sartori, R., 2003. The Thyrrhenian backarc basin and subduction of the Ionian lithosphere. Episodes 26, 217–221.

Schafer, K., Kraft, K.-H., Hausler, H., and Erdmann, J., 1980. In situ stress and palaeostresses in Libya. In: The Geology of Libya (eds M.J. Salem and M.T. Busrewil). Academic Press, London, III, 907-922.

Schivardi, R., and Morelli, A., 2009. Surface wave tomography in the European and Mediterranean region. Geophys. J. Int. 177(3), 1050–1066.

Seber, D., Sandvol, E., Sandvol, C., Brindisi, C. and Barazangi, M., 2001. Crustal model for the Middle East and North Africa region: implications for the isostatic compensation mechanism. Geophys. J. Int., 147: 630–638. doi: 10.1046/j.0956-540x.2001.01572.x.

Serpelloni, E., Vannucci, G., Pondrelli, S., Argnani, A., Casula, G., Anzidei, M., Baldi, P., and Gasperini, P., 2007. Kinematics of theWestern Africa–Eurasia plate boundary from focal mechanisms and GPS data. Geophys. J. Int. 169 (3), 1180–1200. doi:10.1111/j.1365-246X.2007.03367.x.

Suleiman, A., and Doser, D., 1995. The seismicity, seismotectonics and earthquake hazards of Libya, with detailed analysis of the 1935 April 19, M = 7.1 earthquake sequence. Geophys J Int 120:312–322

Suckale, J., Rondenay, S., Sachpazi, M., Charalampakis, M., Hosa, A., and Royden, L.H., 2009. High-resolution seismic imaging of the western Hellenic subduction zone using teleseismic scattered waves. Geophys. J. Int. 178, 775–791.

Tedla, G.E., Van der Meijde, M., Nyblade, A.A., and Meer, F.D., 2011. A crustal thickness map of Africa derived from a global gravity field model using Euler deconvolution. Geophysical Journal International 187, 1–9.

Van der Meijde, M., Van der Lee, S., and Giardini, D., 2003. Crustal structure beneath broad-band seismic stations in the Mediterranean region. Geophysical Journal International, 152(3), 729-739.

Van der Meer, F., and Cloetingh, S., 1993. Intraplate stresses and subsidence history of the Sirt Basin (Libya). Tectonophysics, v. 226, p. 37-58

Van der Meijde, M., van der Lee, S., and Giardini, D., 2005. Seismic discontinuities in the Mediterranean mantle. Phys. Earth Planet. Inter., 148, 233–250

Vannucci, G., Pondrelli, S., Argnani, A., Morelli, A., Gasperini, P., and Boschi, E., 2004. An atlas of Mediterranean seismicity. Annals of Geophysics, 47 (1): 247-306 Suppl. S, FEB 2004

Vavryčuk, V., 2014. Iterative joint inversion for stress and fault orientations from focal mechanisms. Geophysical Journal International, 199, 69-77, doi: 10.1093/gji/ggu224.

Viti, M., Mantovani, E., Babbucci, D. and Tamburelli, C., 2011. Plate kinematics and geodynamics in the central Mediterranean. J. Geodyn, 51, 190-204, doi: 10.1016/j.jog.2010.02.006.

Ward, S.N., 1994. Constraints on the seismotectonics of the central Mediterranean from Very Long Baseline Interferometry. Geophys. J. Int. 117, 441–452.

Westaway, R., 1990. The Tripoli, Libya, earthquake of September 4, 1974: implications for the active tectonics of the Central Mediterranean. Tectonics, 9, 231–248.

Zandt, G., and Ammon, C.J., 1995. Continental Crustal composition constrained by measurements of crustal Poisson's ratio. Nature, 374, 152-154.

APPENDIX

Regional events used for surface wave dispersion study.

No	Event ID	Source	DATE	TIME	LAT	LON	DEPTH	MAG
1	7396000	ISC	2005-08-04	10:45:28.68	34.8334	26.5067	10.0	m_b4.7
2	7703572	ISC	2005-10-11	05:44:26.35	35.4036	27.5144	18.1	m_b 4.8
3	8096168	ISC	2006-02-22	05:38:26.21	35.1776	27.1521	33.2	m_b 4.6
4	10603507	ISC	2006-03-14	09:16:58.47	37.7928	19.8812	10.0	m_b 4.7
5	10697645	ISC	2006-04-09	27:19.53:00	35.1753	27.2497	30.6	m_b 5.1
6	10697787	ISC	2006-04-15	21:15:10.95	37.5772	20.9658	10.0	m_b 4.9
7	10697808	ISC	2006-04-17	02:44:06.43	39.6131	17.1190	10.0	m_b 4.7
8	8320736	ISC	2006-04-18	03:54:33.42	37.5222	20.9650	10.0	m_b 4.5
9	10697860	ISC	2006-04-19	15:16:23.91	37.6366	20.8928	10.0	m_b 5.0
10	9436148	ISC	2006-05-29	02:20:06.88	41.8505	15.8858	26.4	m_b 4.8
11	8474917	ISC	2006-06-17	12:14:00.21	34.2584	25.0788	29.5	m_b 4.6
12	10699925	ISC	2006-08-16	19:17:51.29	34.2652	26.4918	29.5	m_b 4.7
13	11122076	ISC	2006-10-12	13:31:02.57	34.3370	26.5794	32.5	m_b 4.7
14	8823487	ISC	2006-10-24	03:39:38.73	35.0658	27.1942	39.3	m_b 4.6
15	10389115	ISC	2007-01-18	22:25:20.74	34.7423	22.5845	18.8	m_b 4.8
16	11499971	ISC	2007-02-10	09:12:56.69	35.3833	21.3521	23.2	m_b 4.9
17	11501161	ISC	2007-02-12	10:37:41.30	40.4930	15.6080	07.9	m_b 1.6
18	11921336	ISC	2007-04-10	7:11:29:00	38.4900	22.0000	31.0	M_D 3.1
19	12691213	ISC	2007-06-29	18:09:13:00	39.2973	20.2486	17.6	m_b 5.3
20	13200323	ISC	2007-08-12	11:20:43.69	39.3347	20.2228	12.4	m_b 4.5
21	13202361	ISC	2007-08-27	06:29:03.70	38.2400	20.4184	13.3	m_b 4.6
22	13204037	ISC	2007-09-24	18:12:31.52	34.7734	23.3646	31.7	m_b 5.0
23	13241909	ISC	2007-10-14	09:18:10.47	34.3651	26.5943	23.1	m_b 4.6
24	13250441	ISC	2007-10-27	5:29:40:00	37.6993	21.2513	10.0	m_b 4.9
25	14234544	ISC	2008-02-21	05:00:08.26	37.7401	17.9620	40.8	m_b 4.2
26	10980071	ISC	2008-02-14	12:00:26:00	40.4774	33.3412	03.9	m_b 3.0
27	13482221	ISC	2008-03-05	16:11:35.12	36.1023	27.4740	10.0	m_b 4.8
28	13482228	ISC	2008-03-05	16:14:39.39	36.0719	27.4222	10.0	m_b 4.8
29	13483853	ISC	2008-03-07	20:28:23.75	36.1150	21.8596	07.7	m_b 4.7
30	13488408	ISC	2008-03-14	07:10:23.75	36.0052	21.8707	10.0	m_b 4.7
31	13496162	ISC	2008-03-25	04:26:26.77	36.2548	21.6866	10.2	m_b 4.6
32	13224849	ISC	2008-04-12	07:58:33.34	34.1040	25.4108	13.9	m_b 4.5
33	13231364	ISC	2008-06-08	12:25:30:00	37.9608	21.4486	15.8	m_b 6.0
34	13378187	ISC	2008-06-21	05:57:15.20	36.0321	21.8502	10.0	m_b 4.9
35	13378208	ISC	2008-06-21	11:36:25:00	36.0663	21.9630	23.6	m_b 5.4
36	13656608	ISC	2008-07-01	14:42:56.10	43.4390	12.9890	07.8	m_b 1.5
37	13390413	ISC	2008-07-30	5:02:58:00	38.1027	20.1788	04.9	m_b 4.8
38	13392641	ISC	2008-08-26	09:46:27.26	36.1204	21.7672	39.1	m_b 4.4
39	13396984	ISC	2008-10-14	02:17:01:00	38.8061	23.5997	40.0	m_b 4.5
40	13898444	ISC	2008-10-23	09:34:57.10	42.0380	12.9980	10.0	m_b 2.1
41	12073142	ISC	2008-11-11	06:04:52.30	36.0989	21.8658	10.0	m_b 4.0
42	13399850	ISC	2008-11-11	16:17:01.65	34.1950	25.0737	29.1	m_b 4.6

No	Event ID	Source	DATE	TIME	LAT	LON	DEPTH	MAG
43	15699501	ISC	2009-01-19	23:02:05.55	34.6544	24.8753	14.8	m_b 4.7
44	13434691	ISC	2009-02-16	23:16:39:00	37.2403	20.9006	13.2	m_b 5.5
45	12702301	ISC	2009-03-02	22:01:10.29	36.6894	26.6419	11.8	m_b 3.2
46	12025785	ISC	2009-03-19	14:15:18.28	35.0866	23.4280	29.9	m_b 5.1
47	12934692	ISC	2009-04-06	1:36:30:00	42.3661	13.3496	07.4	m_b 4.6
48	14836959	ISC	2009-04-06	23:17:33:00	42.2660	13.4990	09.8	M_L 2.6
49	14835675	ISC	2009-04-06	03:53:34.70	42.3730	13.3340	10.0	M_L 2.7
50	14837580	ISC	2009-04-07	17:48:42:00	42.3580	13.5310	10.6	M_L 3.3
51	16194316	ISC	2009-04-09	0:53:02:00	42.4987	13.3468	13.6	m_b 5.2
52	13438508	ISC	2009-04-14	06:14:19.33	34.2405	23.8392	39.1	m_b 4.5
53	13438687	ISC	2009-04-16	14:25:31.08	34.1743	25.0855	21.4	m_b 4.7
54	14844013	ISC	2009-04-18	19:25:13.90	42.3720	13.3560	10.2	m_b 1.5
55	13439125	ISC	2009-04-27	11:52:13.69	36.1054	21.4969	21.3	m_b 3.9
56	12828760	ISC	2009-05-17	11:59:04.34	38.1194	22.6944	13.9	m_b 4.8
57	13197437	ISC	2009-06-19	14:05:00.55	35.3441	28.4806	39.0	m_b 5.5
58	14306606	ISC	2009-06-26	22:14:53.35	36.5237	25.4964	13.4	m_b 4.7
59	13324939	ISC	2009-07-03	04:16:47.33	34.0570	25.6035	26.1	m_b 4.3
60	13324941	ISC	2009-07-03	04:42:33.85	34.6582	24.1274	46.0	m_b 4.6
61	13361331	ISC	2009-07-07	00:32:45.78	34.0305	25.1931	15.7	m_b 4.9
62	13361335	ISC	2009-07-07	01:02:48.14	34.0843	25.5865	17.8	m_b 4.8
63	13763326	ISC	2009-07-07	02:04:03.31	34.0808	25.4920	05.9	m_b 3.9
64	13363385	ISC	2009-07-08	06:19:57.04	34.0197	25.4253	19.4	m_b 4.6
65	13545416	ISC	2009-07-09	16:27:42.14	34.1005	25.5382	19.7	m_b 4.6
66	13381238	ISC	2009-07-11	13:48:47.90	33.9680	25.4127	15.4	m_b 4.3
67	13548900	ISC	2009-08-06	04:57:44.82	37.5053	22.0194	10.6	m_b 4.6
68	15068833	ISC	2009-09-26	13:41:46.00	36.0300	21.9400	08.0	M_D 3.3

DISPERSION CURVES

These curves were used in analysis of uncertainties using clusters of events.

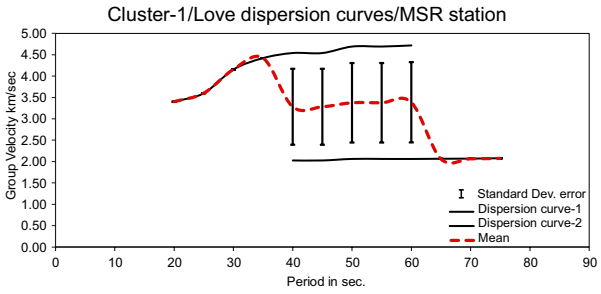

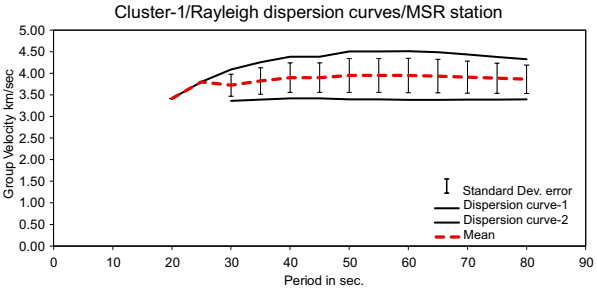

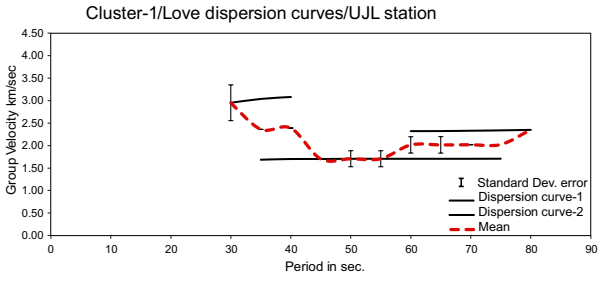

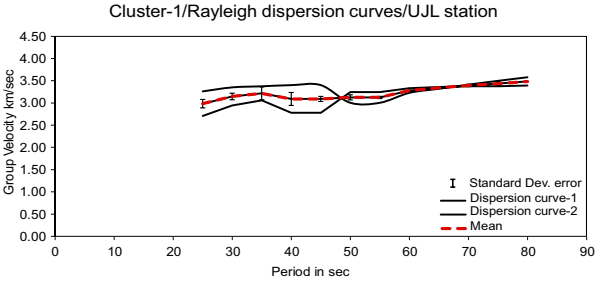

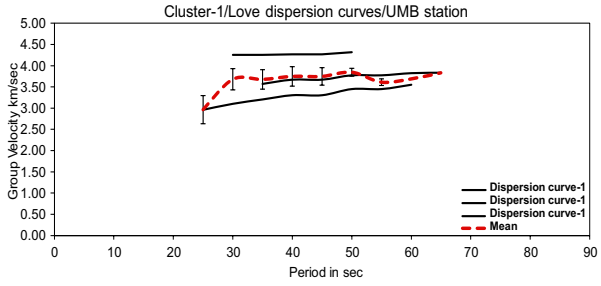

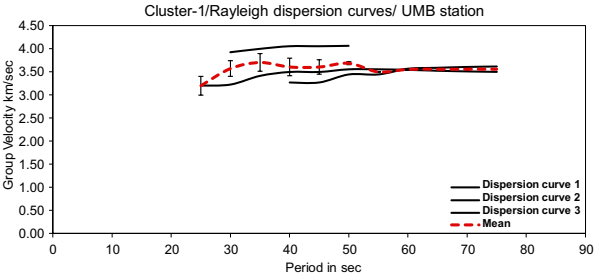

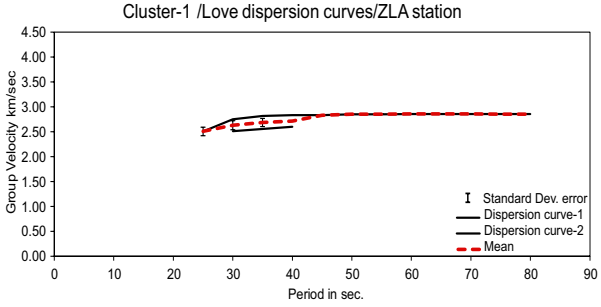

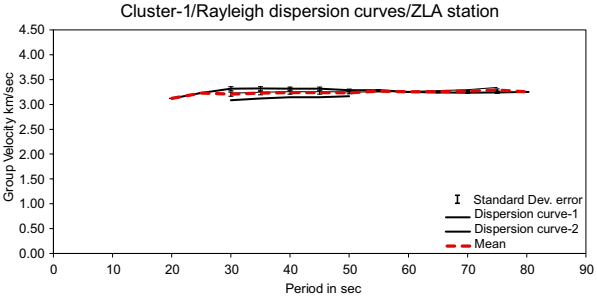

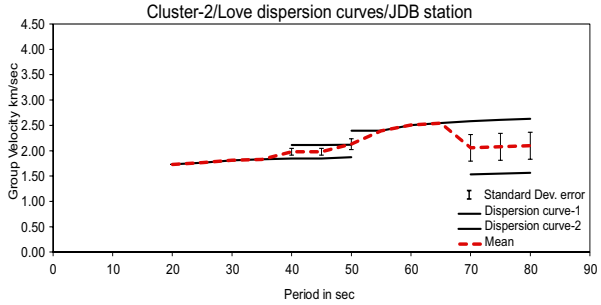

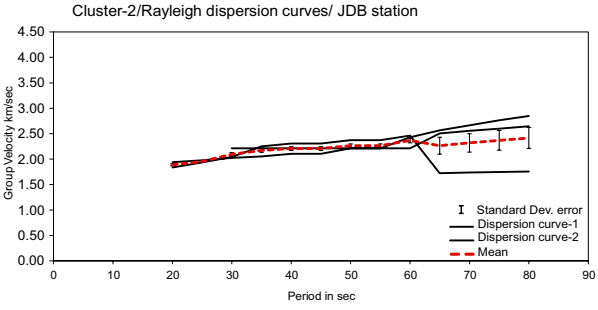

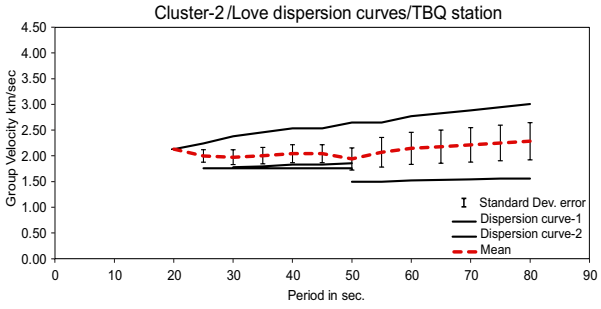
Cluster-2 /Love dispersion curves/TBQ station
Group Velocity km/sec
Period in sec.
Standard Dev. error
Dispersion curve-1
Dispersion curve-2
Mean

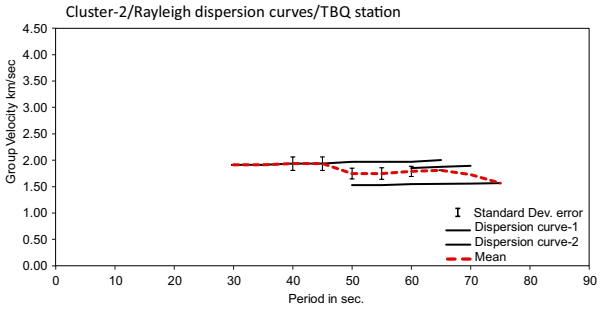
Cluster-2/Rayleigh dispersion curves/TBQ station
Group Velocity km/sec
Period in sec.
Standard Dev. error
Dispersion curve-1
Dispersion curve-2
Mean

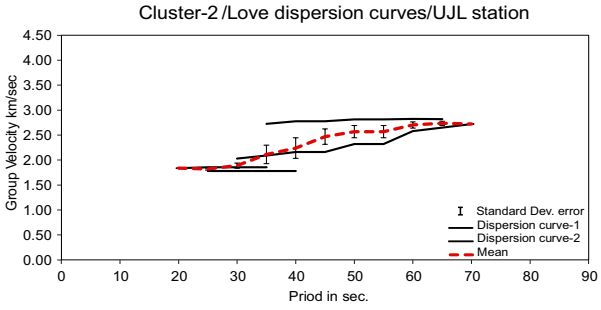
Cluster-2 /Love dispersion curves/UJL station
Group Velocity km/sec
Priod in sec.
Standard Dev. error
Dispersion curve-1
Dispersion curve-2
Mean

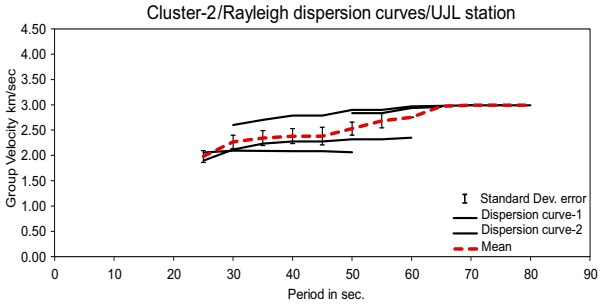
Cluster-2/Rayleigh dispersion curves/UJL station
Group Velocity km/sec
Period in sec.
Standard Dev. error
Dispersion curve-1
Dispersion curve-2
Mean

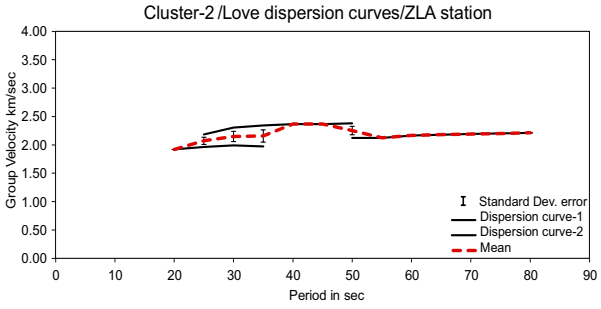
Cluster-2 /Love dispersion curves/ZLA station
Group Velocity km/sec
Period in sec
Standard Dev. error
Dispersion curve-1
Dispersion curve-2
Mean

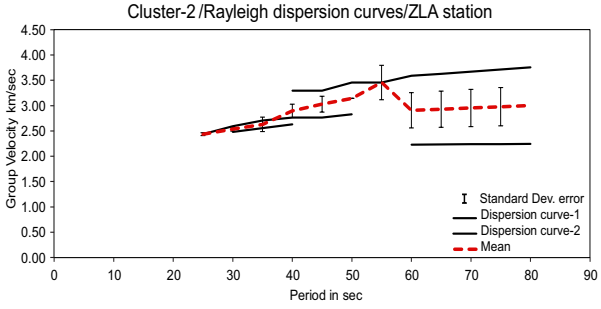
Cluster-2 /Rayleigh dispersion curves/ZLA station
Group Velocity km/sec
Period in sec
Standard Dev. error
Dispersion curve-1
Dispersion curve-2
Mean

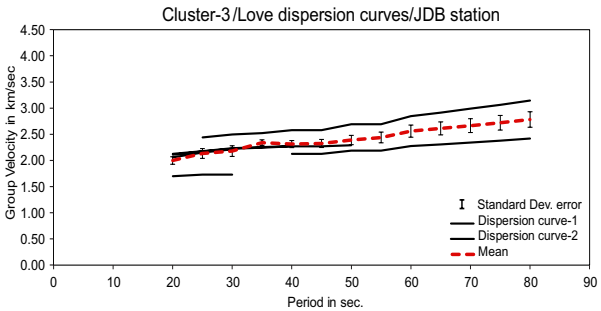
Cluster-3 /Love dispersion curves/JDB station
Group Velocity in km/sec
Period in sec.
Standard Dev. error
Dispersion curve-1
Dispersion curve-2
Mean

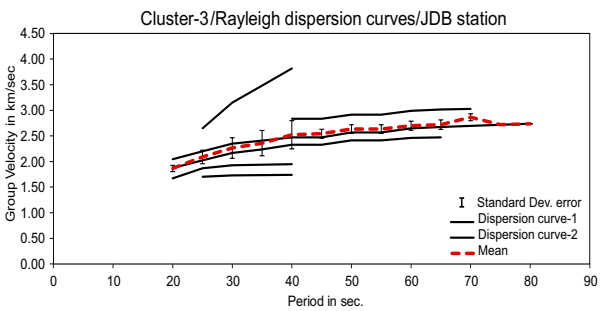
Cluster-3/Rayleigh dispersion curves/JDB station
Group Velocity in km/sec
Period in sec.
Standard Dev. error
Dispersion curve-1
Dispersion curve-2
Mean

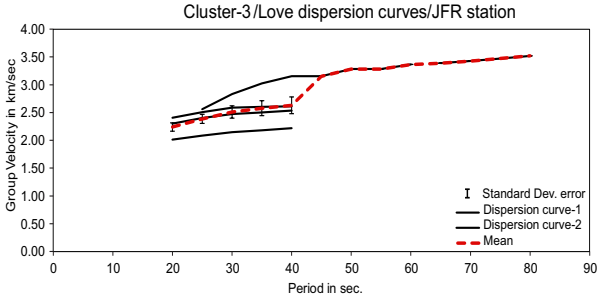
Cluster-3 /Love dispersion curves/JFR station
Group Velocity in km/sec
Period in sec.
Standard Dev. error
Dispersion curve-1
Dispersion curve-2
Mean

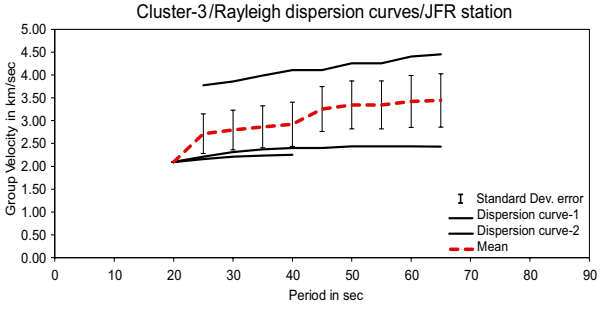
Cluster-3 /Rayleigh dispersion curves/JFR station
Group Velocity in km/sec
Period in sec
Standard Dev. error
Dispersion curve-1
Dispersion curve-2
Mean

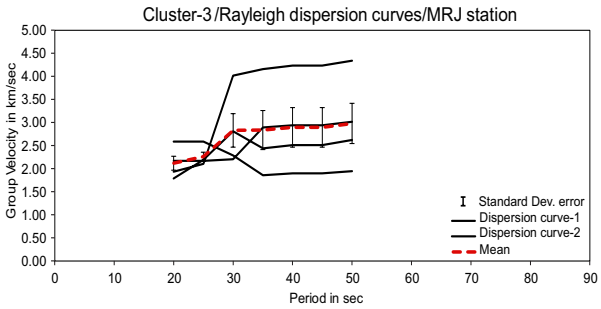
Cluster-3 /Rayleigh dispersion curves/MRJ station
Group Velocity in km/sec
Period in sec
Standard Dev. error
Dispersion curve-1
Dispersion curve-2
Mean

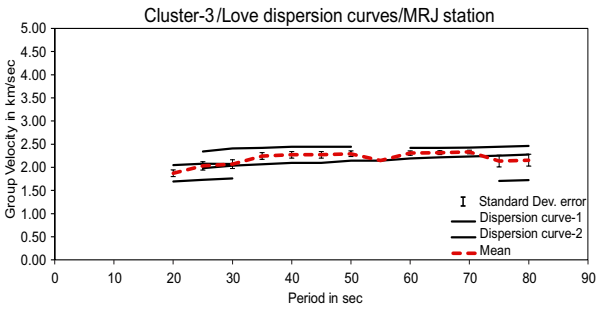
Cluster-3 /Love dispersion curves/MRJ station
Group Velocity in km/sec
Period in sec
Standard Dev. error
Dispersion curve-1
Dispersion curve-2
Mean

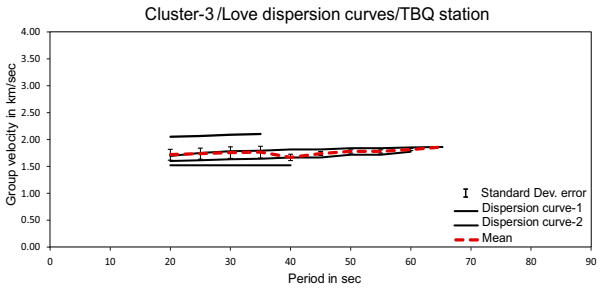
Cluster-3 /Love dispersion curves/TBQ station
Group velocity in km/sec
Period in sec
Standard Dev. error
Dispersion curve-1
Dispersion curve-2
Mean

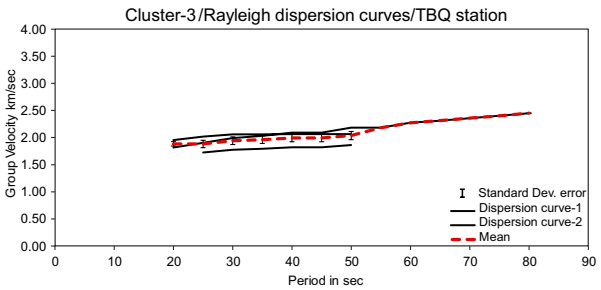
Cluster-3 /Rayleigh dispersion curves/TBQ station
Group Velocity km/sec
Period in sec
Standard Dev. error
Dispersion curve-1
Dispersion curve-2
Mean

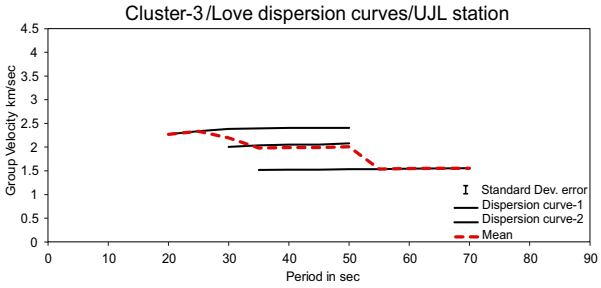
Cluster-3 /Love dispersion curves/UJL station
Group Velocity km/sec
Period in sec
Standard Dev. error
Dispersion curve-1
Dispersion curve-2
Mean

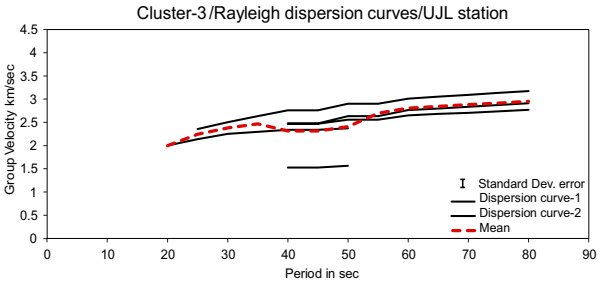
Cluster-3 /Rayleigh dispersion curves/UJL station
Group Velocity km/sec
Period in sec
Standard Dev. error
Dispersion curve-1
Dispersion curve-2
Mean

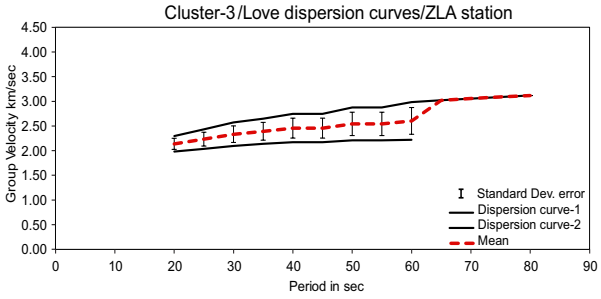
Cluster-3 /Love dispersion curves/ZLA station
Group Velocity km/sec
Period in sec
Standard Dev. error
Dispersion curve-1
Dispersion curve-2
Mean

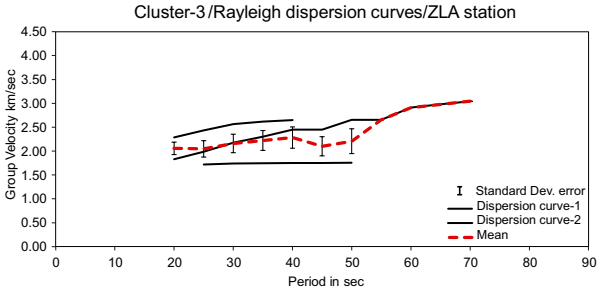
Cluster-3 /Rayleigh dispersion curves/ZLA station
Group Velocity km/sec
Period in sec
Standard Dev. error
Dispersion curve-1
Dispersion curve-2
Mean

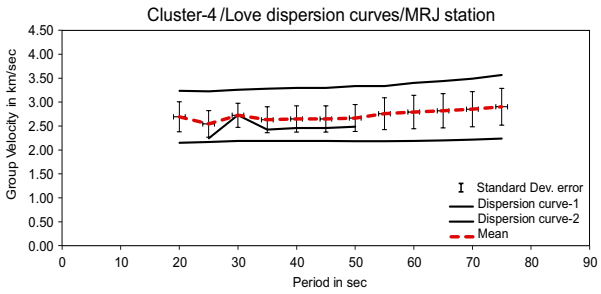
Cluster-4 /Love dispersion curves/MRJ station
Group Velocity in km/sec
Period in sec
Standard Dev. error
Dispersion curve-1
Dispersion curve-2
Mean

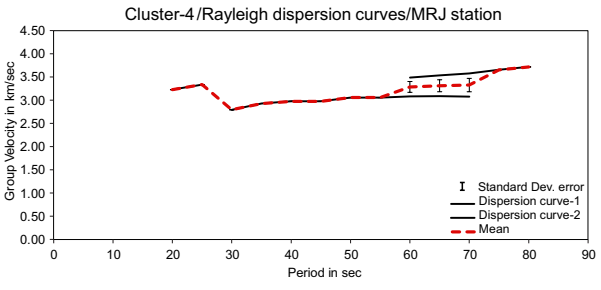
Cluster-4 /Rayleigh dispersion curves/MRJ station
Group Velocity in km/sec
Period in sec
Standard Dev. error
Dispersion curve-1
Dispersion curve-2
Mean

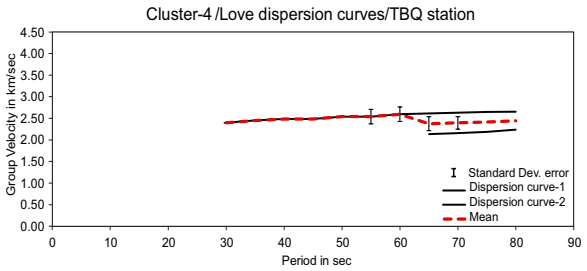
Cluster-4 /Love dispersion curves/TBQ station
Group Velocity in km/sec
Period in sec
Standard Dev. error
Dispersion curve-1
Dispersion curve-2
Mean

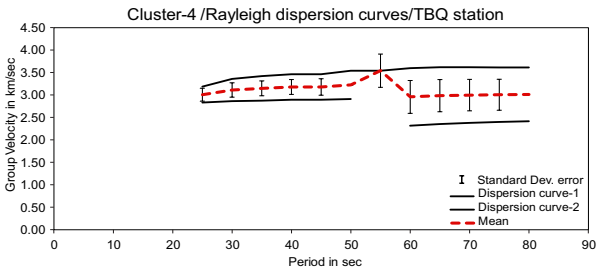
Cluster-4 /Rayleigh dispersion curves/TBQ station
Group Velocity in km/sec
Period in sec
Standard Dev. error
Dispersion curve-1
Dispersion curve-2
Mean

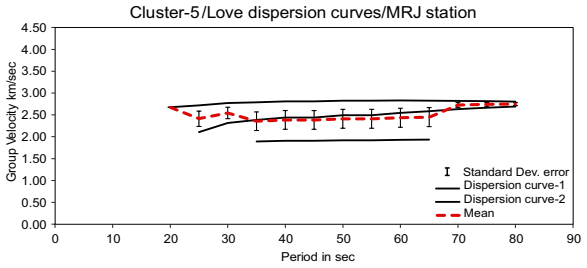
Cluster-5 /Love dispersion curves/MRJ station
Group Velocity km/sec
Period in sec
Standard Dev. error
Dispersion curve-1
Dispersion curve-2
Mean

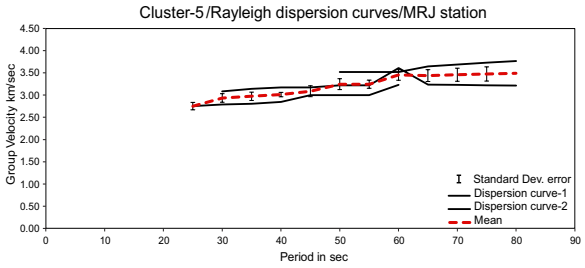
Cluster-5 /Rayleigh dispersion curves/MRJ station
Group Velocity km/sec
Period in sec
Standard Dev. error
Dispersion curve-1
Dispersion curve-2
Mean

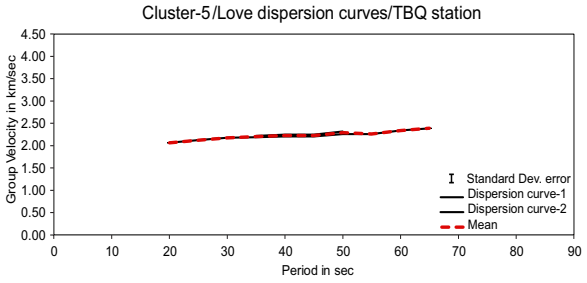
Cluster-5 /Love dispersion curves/TBQ station
Group Velocity in km/sec
Period in sec
Standard Dev. error
Dispersion curve-1
Dispersion curve-2
Mean

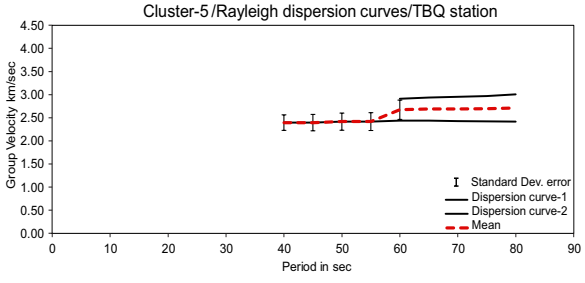
Cluster-5 /Rayleigh dispersion curves/TBQ station
Group Velocity km/sec
Period in sec
Standard Dev. error
Dispersion curve-1
Dispersion curve-2
Mean

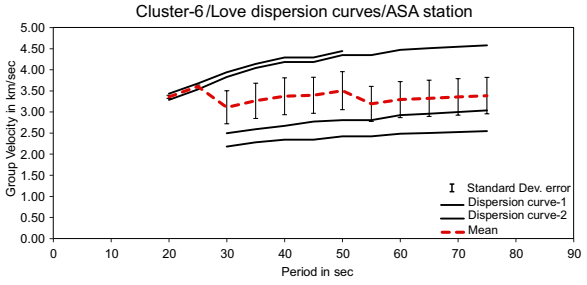
Cluster-6 /Love dispersion curves/ASA station
Group Velocity in km/sec
Period in sec
Standard Dev. error
Dispersion curve-1
Dispersion curve-2
Mean

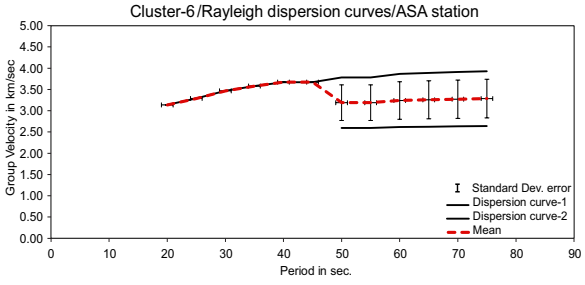
Cluster-6 /Rayleigh dispersion curves/ASA station
Group Velocity in km/sec
Period in sec.
Standard Dev. error
Dispersion curve-1
Dispersion curve-2
Mean

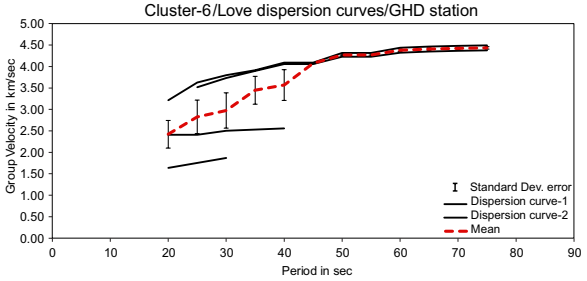
Cluster-6 /Love dispersion curves/GHD station
Group Velocity in km/sec
Period in sec
Standard Dev. error
Dispersion curve-1
Dispersion curve-2
Mean

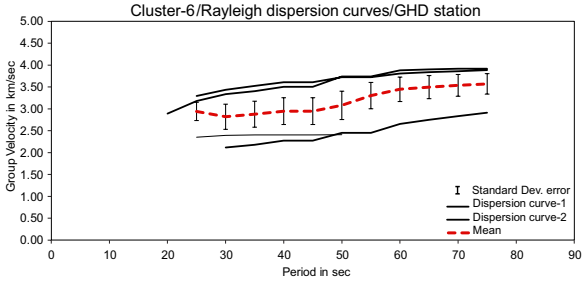
Cluster-6 /Rayleigh dispersion curves/GHD station
Group Velocity in km/sec
Period in sec
Standard Dev. error
Dispersion curve-1
Dispersion curve-2
Mean

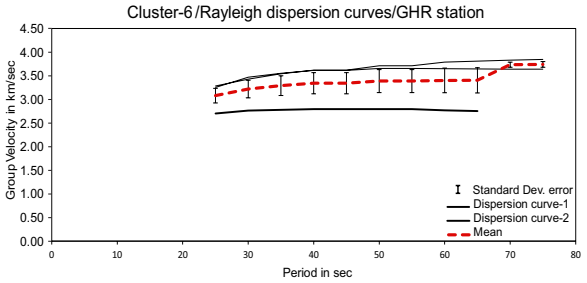
Cluster-6 /Rayleigh dispersion curves/GHR station
Group Velocity in km/sec
Period in sec
Standard Dev. error
Dispersion curve-1
Dispersion curve-2
Mean

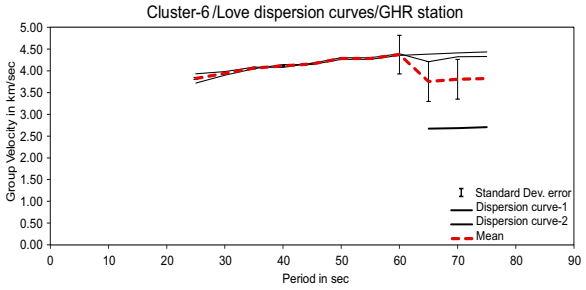
Cluster-6 /Love dispersion curves/GHR station
Group Velocity in km/sec
Period in sec
Standard Dev. error
Dispersion curve-1
Dispersion curve-2
Mean

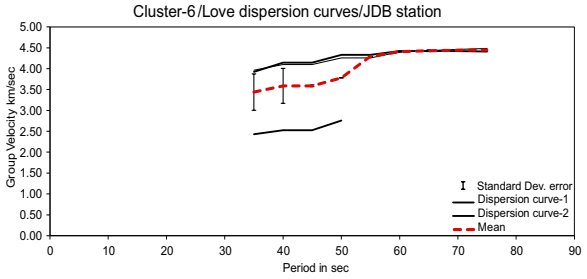
Cluster-6 /Love dispersion curves/JDB station
Group Velocity km/sec
Period in sec
Standard Dev. error
Dispersion curve-1
Dispersion curve-2
Mean

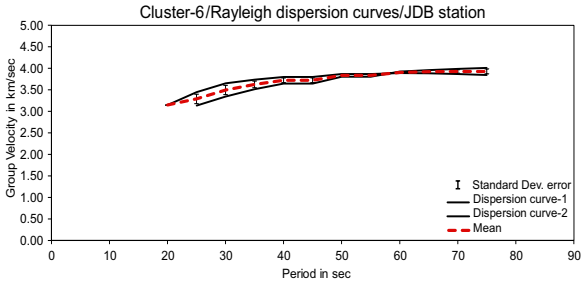
Cluster-6 /Rayleigh dispersion curves/JDB station
Group Velocity in km/sec
Period in sec
Standard Dev. error
Dispersion curve-1
Dispersion curve-2
Mean

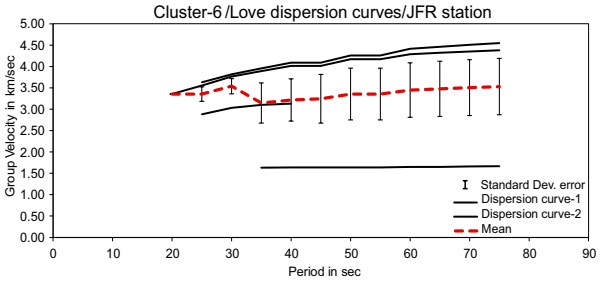
Cluster-6 /Love dispersion curves/JFR station
Group Velocity in km/sec
Period in sec
Standard Dev. error
Dispersion curve-1
Dispersion curve-2
Mean

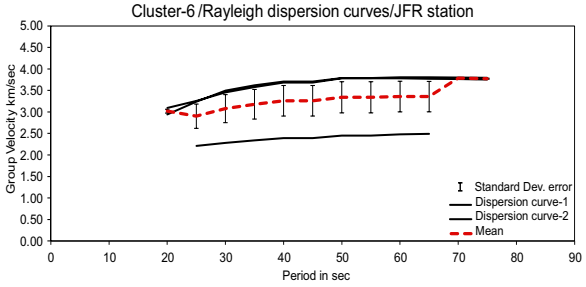
Cluster-6 /Rayleigh dispersion curves/JFR station
Group Velocity km/sec
Period in sec
Standard Dev. error
Dispersion curve-1
Dispersion curve-2
Mean

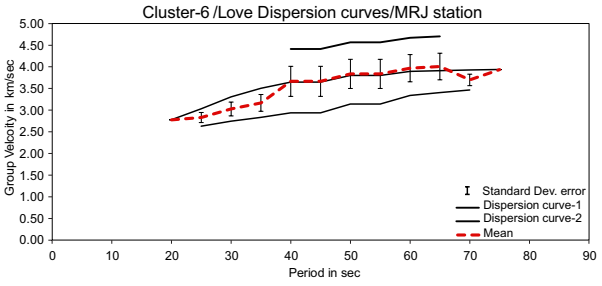
Cluster-6 /Love Dispersion curves/MRJ station
Group Velocity in km/sec
Period in sec
Standard Dev. error
Dispersion curve-1
Dispersion curve-2
Mean

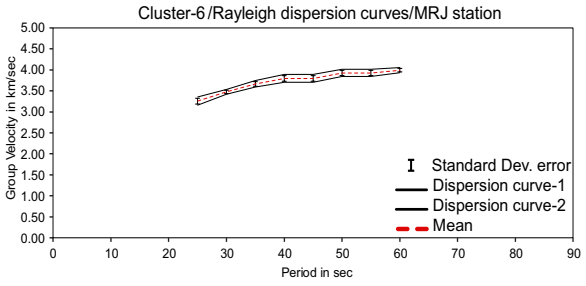
Cluster-6 /Rayleigh dispersion curves/MRJ station
Group Velocity in km/sec
Period in sec
Standard Dev. error
Dispersion curve-1
Dispersion curve-2
Mean

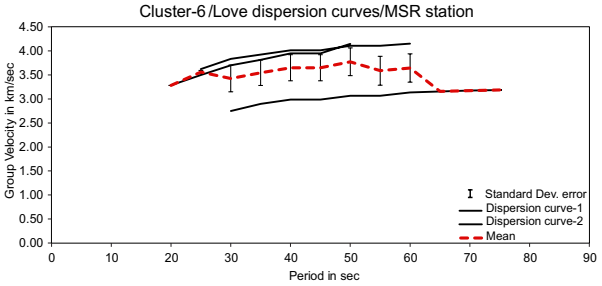
Cluster-6 /Love dispersion curves/MSR station
Group Velocity in km/sec
Period in sec
Standard Dev. error
Dispersion curve-1
Dispersion curve-2
Mean

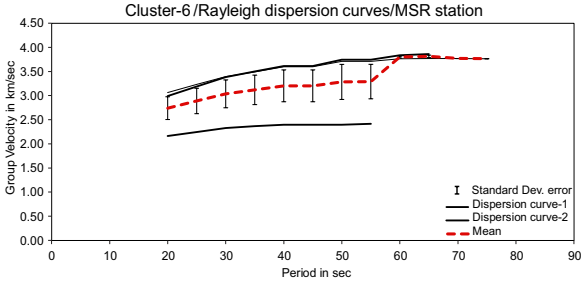
Cluster-6 /Rayleigh dispersion curves/MSR station
Group Velocity in km/sec
Period in sec
Standard Dev. error
Dispersion curve-1
Dispersion curve-2
Mean

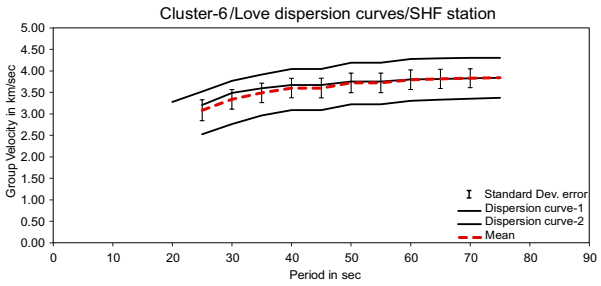
Cluster-6 /Love dispersion curves/SHF station
Group Velocity in km/sec
Period in sec
Standard Dev. error
Dispersion curve-1
Dispersion curve-2
Mean

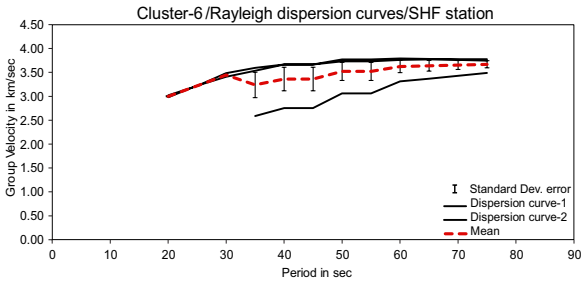
Cluster-6 /Rayleigh dispersion curves/SHF station
Group Velocity in km/sec
Period in sec
Standard Dev. error
Dispersion curve-1
Dispersion curve-2
Mean

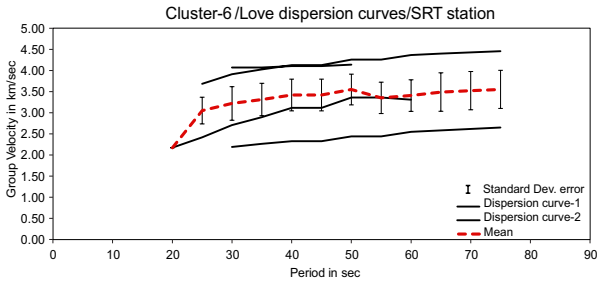
Cluster-6 /Love dispersion curves/SRT station
Group Velocity in km/sec
Period in sec
Standard Dev. error
Dispersion curve-1
Dispersion curve-2
Mean

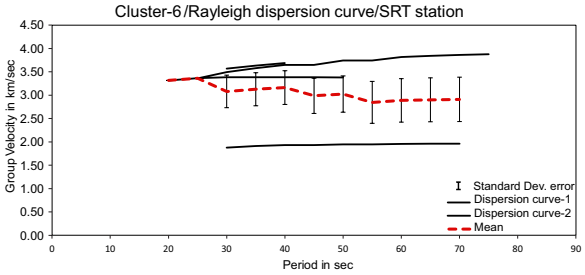
Cluster-6 /Rayleigh dispersion curve/SRT station
Group Velocity in km/sec
Period in sec
Standard Dev. error
Dispersion curve-1
Dispersion curve-2
Mean

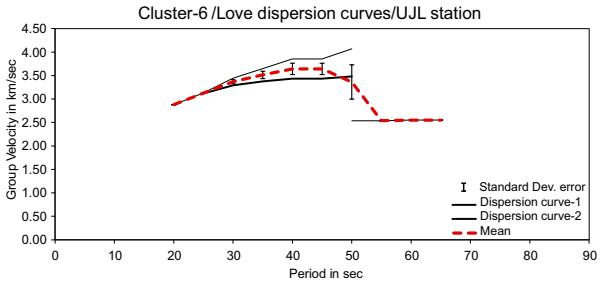
Cluster-6 /Love dispersion curves/UJL station
Group Velocity in km/sec
Period in sec
Standard Dev. error
Dispersion curve-1
Dispersion curve-2
Mean

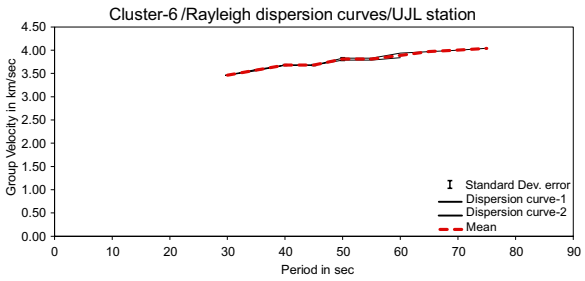
Cluster-6 /Rayleigh dispersion curves/UJL station
Group Velocity in km/sec
Period in sec
Standard Dev. error
Dispersion curve-1
Dispersion curve-2
Mean

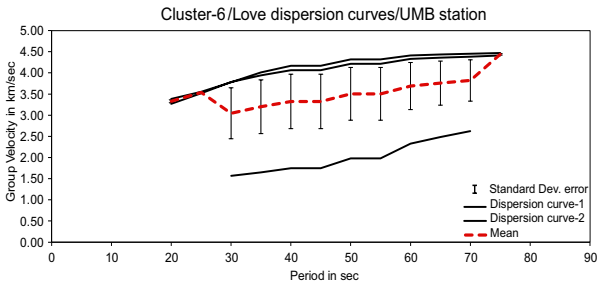
Cluster-6 /Love dispersion curves/UMB station
Group Velocity in km/sec
Period in sec
Standard Dev. error
Dispersion curve-1
Dispersion curve-2
Mean

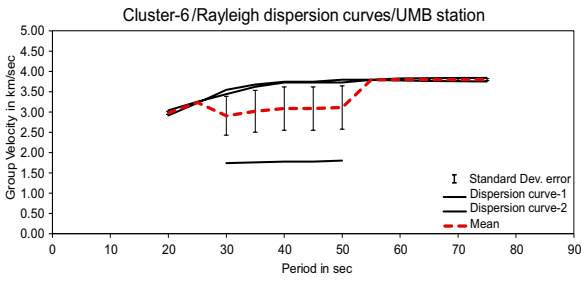
Cluster-6 /Rayleigh dispersion curves/UMB station
Group Velocity in km/sec
Period in sec
Standard Dev. error
Dispersion curve-1
Dispersion curve-2
Mean

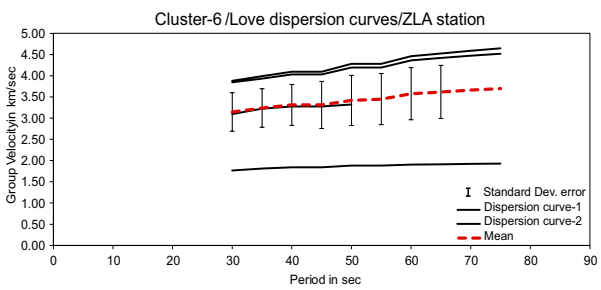
Cluster-6 /Love dispersion curves/ZLA station
Group Velocityin km/sec
Period in sec
Standard Dev. error
Dispersion curve-1
Dispersion curve-2
Mean

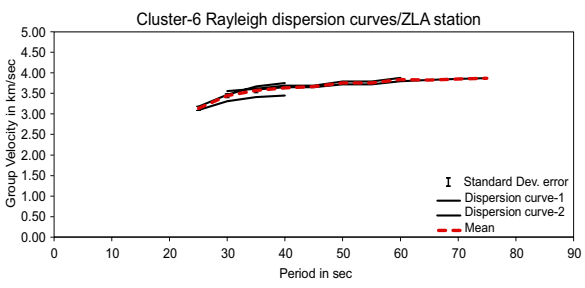
Cluster-6 Rayleigh dispersion curves/ZLA station
Group Velocity in km/sec
Period in sec
Standard Dev. error
Dispersion curve-1
Dispersion curve-2
Mean

FOCAL MECHANISM SOLUTIONS

Different colors indicate different methods for determining fault plane solutions implemented in Seisan (FOCMEC, FTPIT, PINV, and HASH) P=P axis, T=T axis, triangles=T, circles=P). See Seisan manual for details.

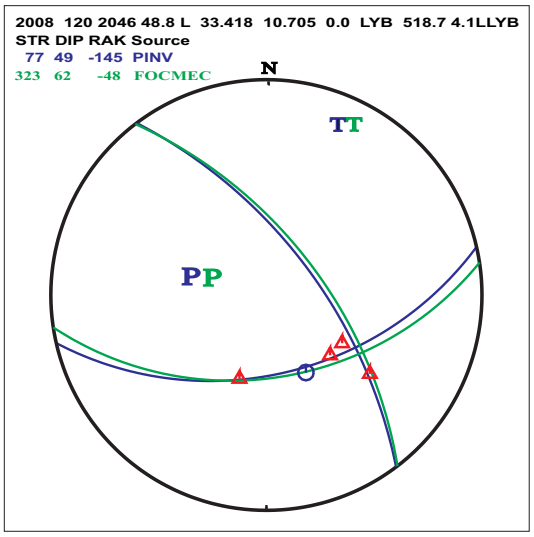

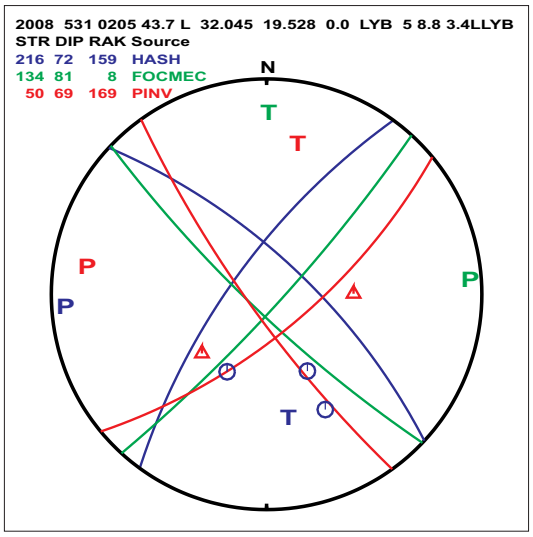

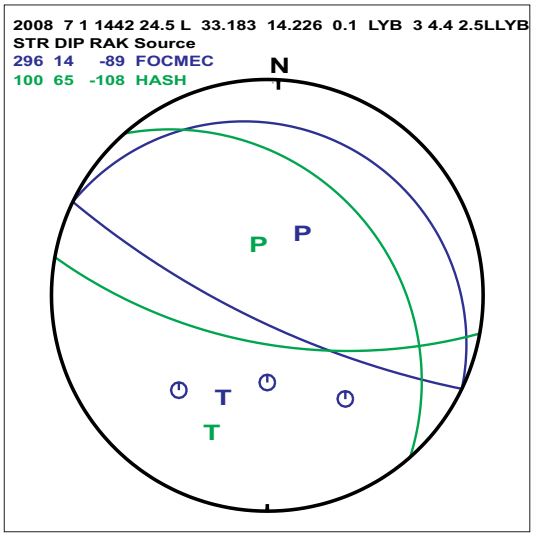

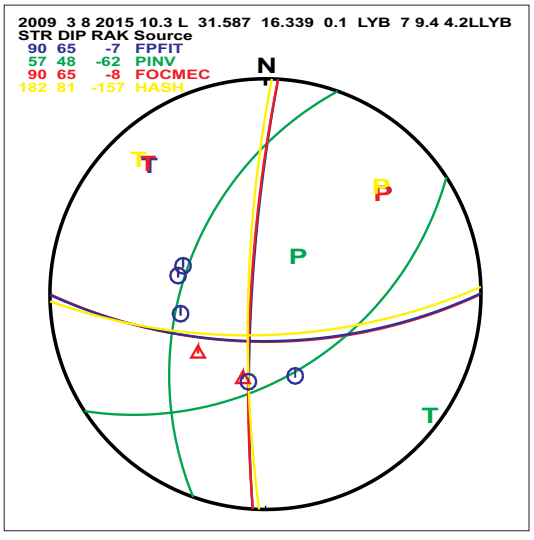

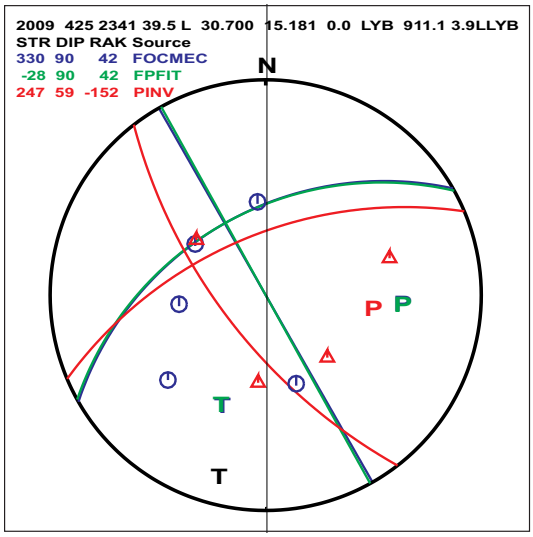
2009 425 2341 39.5 L 30.700 15.181 0.0 LYB 911.1 3.9LLYB
STR DIP RAK Source
330 90 42 FOCMEC
-28 90 42 FPFIT
247 59 -152 PINV
N
P P
T
T

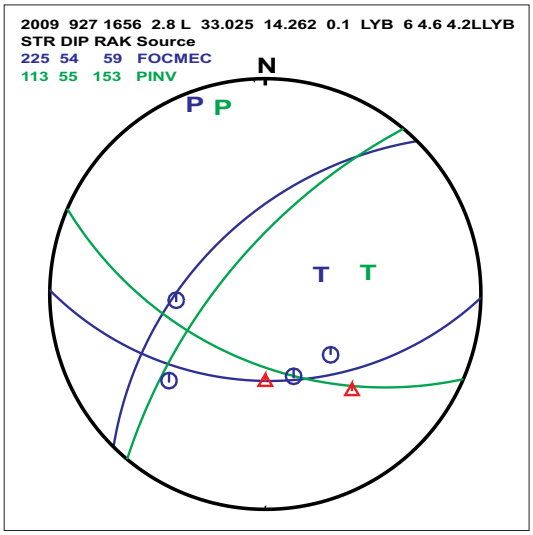
2009 927 1656 2.8 L 33.025 14.262 0.1 LYB 6 4.6 4.2LLYB
STR DIP RAK Source
225 54 59 FOCMEC
113 55 153 PINV
N
P P
T T

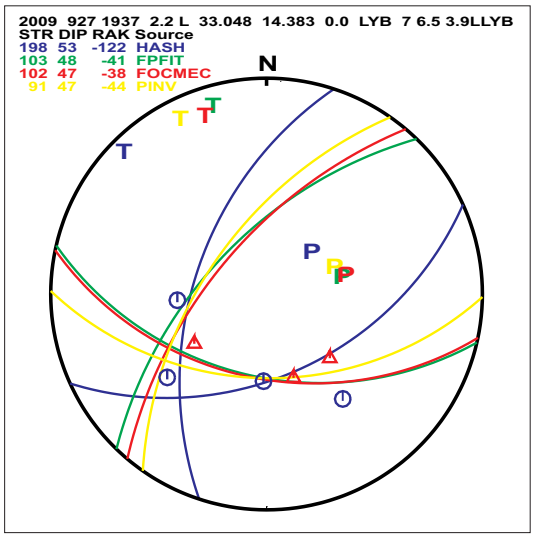
2009 927 1937 2.2 L 33.048 14.383 0.0 LYB 7 6.5 3.9LLYB
STR DIP RAK Source
198 53 -122 HASH
103 48 -41 FPFIT
102 47 -38 FOCMEC
91 47 -44 PINV
N
T T T
T
P
P P

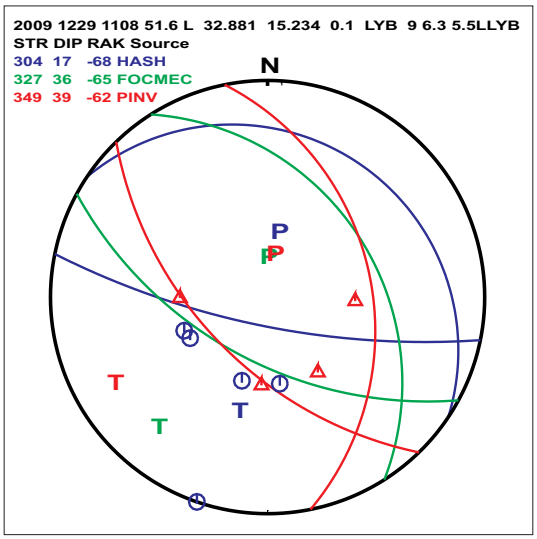
2009 1229 1108 51.6 L 32.881 15.234 0.1 LYB 9 6.3 5.5LLYB
STR DIP RAK Source
304 17 -68 HASH
327 36 -65 FOCMEC
349 39 -62 PINV
N
P
P
T
T
T

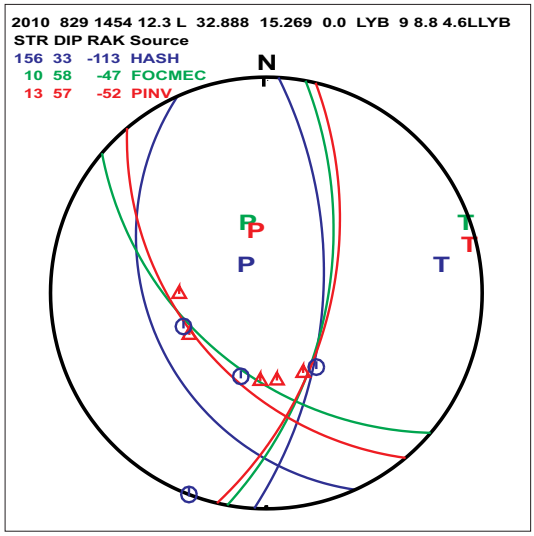
2010 829 1454 12.3 L 32.888 15.269 0.0 LYB 9 8.8 4.6LLYB
STR DIP RAK Source
156 33 -113 HASH
10 58 -47 FOCMEC
13 57 -52 PINV
N
P P
P
T
T
T

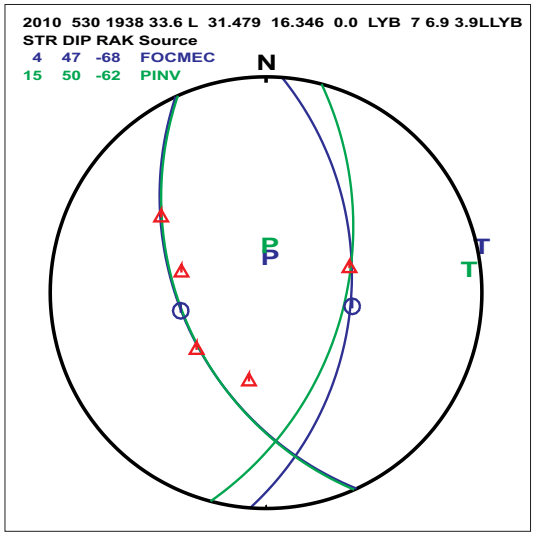
2010 530 1938 33.6 L 31.479 16.346 0.0 LYB 7 6.9 3.9LLYB
STR DIP RAK Source
4 47 -68 FOCMEC
15 50 -62 PINV
N
P
P
T
T

VITA

Abdusalam A. Agail was born in 1978 in small city on the Mediterranean S.Khamis-Alkhoms, Libya. Abdusalam is the second son of the family of Ali Agail and Salmah Alabed. He finished high school in 1996 and started his bachelor`s degree at the College of Science-University of Elmergib, Department of Geology and Environmental Sciences. He gradated with honors in 2000 and later he got an offer to work for the General Water Authority (GWA) Tripoli, Libya. Abdusalam's main duties were supervising the drilling of water wells and writing technical reports as well as signing drilling contracts.

In 2005 he got an offer to work as teaching assistant at the University of Elmergib. He taught different introductory laboratory courses including sedimentology, field geology, paleontology, and petroleum geology. In 2007 he was granted a scholarship from the University to pursue a Master`s degree in Geology. Later in 2008 he moved to the United States and started his Master`s program in 2009 at the University of Texas at El Paso-Department of Geological Sciences. He graduated with his M.S. in 2011. His thesis title was "Nummulites Biofabrics as tool for quality evaluation of the Eocene Jdeir formation Reservoir offshore, Libya". Later in 2011 he started his PhD program at the University of Texas-Department of Geological Sciences.

Permanent address:
P.O.Box: 40169.
Al-Khoms-LIBYA

Abdusalam Ali Agail. El Paso, Texas
October 18, 2015